Cell Reports

Article

The Interaction of the Tumor Suppressor FAM46C with p62 and FNDC3 Proteins Integrates Protein and Secretory Homeostasis

Graphical Abstract

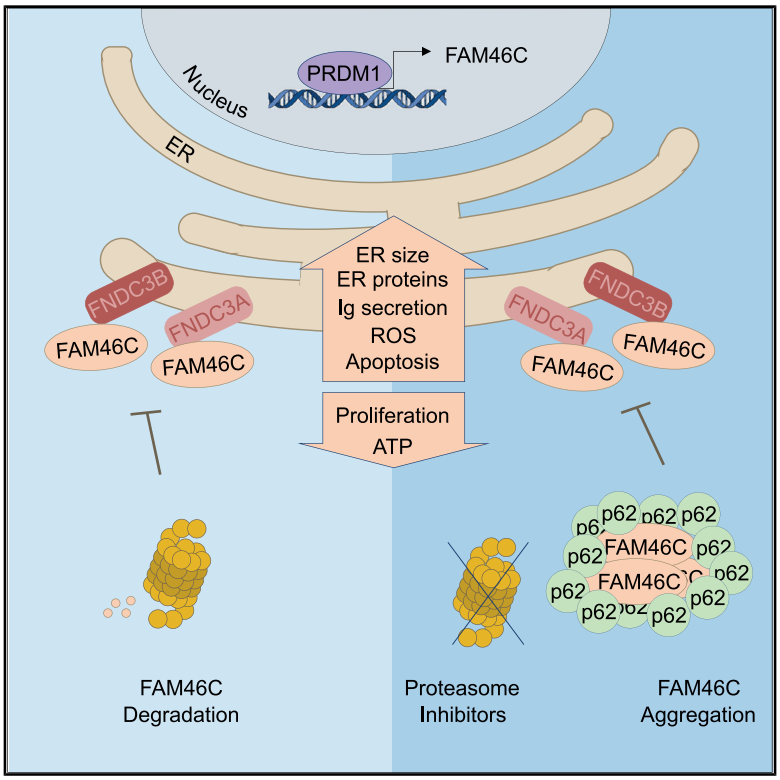

Highlights

- In myeloma cells, FAM46C boosts ER growth and Ig secretion beyond sustainability
- The ER-expanding activity of FAM46C requires its interaction with FNDC3 proteins
- FAM46C abundance is tightly regulated by UPS-operated proteolysis
- p62 compensates for UPS insufficiency by sequestering FAM46C away from the ER

Authors

Chiara Fucci, Massimo Resnati, Elena Riva, ..., Luca Rampoldi, Simone Cenci, Enrico Milan

Correspondence

cenci.simone@hsr.it (S.C.), milan.enrico@hsr.it (E.M.)

In Brief

Fucci et al. show that the poly(A) polymerase FAM46C acts as a multiple myeloma-specific tumor suppressor, increasing secretory capacity and antibody production beyond sustainability via its interaction with endoplasmic reticulum transmembrane FNDC3 proteins. Moreover, its activity is restricted through proteasomal degradation or p62-dependent aggregation and sequestration from FNDC3 proteins.

Fucci et al., 2020, Cell Reports *32*, 108162
September 22, 2020
https://doi.org/10.1016/j.celrep.2020.108162

CellPress

Cell Reports

CellPress
OPEN ACCESS

Article

The Interaction of the Tumor Suppressor FAM46C with p62 and FNDC3 Proteins Integrates Protein and Secretory Homeostasis

Chiara Fucci,[1] Massimo Resnati,[1] Elena Riva,[1] Tommaso Perini,[1,2] Elena Ruggieri,[1,2] Ugo Orfanelli,[1] Francesca Paradiso,[1] Floriana Cremasco,[1] Andrea Raimondi,[3] Elena Pasqualetto,[4] Mario Nuvolone,[5] Luca Rampoldi,[4] Simone Cenci,[1,2,6,7,*] and Enrico Milan[1,2,6,7,8,*]

[1]Age Related Diseases Unit, Division of Genetics and Cell Biology, San Raffaele Scientific Institute, 20132 Milan, Italy
[2]University Vita-Salute San Raffaele, 20132 Milan, Italy
[3]Experimental Imaging Center, Advanced Light and Electron Microscopy BioImaging Center, San Raffaele Scientific Institute, 20132 Milan, Italy
[4]Molecular Genetics of Renal Disorders Unit, Division of Genetics and Cell Biology, San Raffaele Scientific Institute, 20132 Milan, Italy
[5]Amyloidosis Research and Treatment Center, Foundation IRCCS Policlinico San Matteo, 27100 Pavia, Italy
[6]Senior author
[7]These authors contributed equally
[8]Lead Contact
*Correspondence: cenci.simone@hsr.it (S.C.), milan.enrico@hsr.it (E.M.)
https://doi.org/10.1016/j.celrep.2020.108162

SUMMARY

FAM46C is a non-canonical poly(A) polymerase uniquely mutated in up to 20% of multiple myeloma (MM) patients, implying a tissue-specific tumor suppressor function. Here, we report that FAM46C selectively stabilizes mRNAs encoding endoplasmic reticulum (ER)-targeted proteins, thereby concertedly enhancing the expression of proteins that control ER protein import, folding, N-glycosylation, and trafficking and boosting protein secretion. This role requires the interaction with the ER membrane resident proteins FNDC3A and FNDC3B. In MM cells, FAM46C expression raises secretory capacity beyond sustainability, inducing ROS accumulation, ATP shortage, and cell death. FAM46C activity is regulated through rapid proteasomal degradation or the inhibitory interaction with the ZZ domain of the autophagic receptor p62 that hinders its association with FNDC3 proteins via sequestration in $p62^{+}$ aggregates. Altogether, our data disclose a p62/FAM46C/FNDC3 circuit coordinating sustainable secretory activity and survival, providing an explanation for the MM-specific oncosuppressive role of FAM46C and uncovering potential therapeutic opportunities against cancer.

INTRODUCTION

Multiple myeloma (MM) is a plasma cell (PC) tumor responsible for 2% of all cancer deaths. PCs are the terminal effectors of the B lymphocyte lineage in charge of immunoglobulin (Ig) production. The intensive proteosynthetic activity results in abundant misfolded by-products, causing a critical addiction of normal and malignant PCs on protein-degradative pathways: the ubiquitin-proteasome system (UPS) and macroautophagy, usually referred to as autophagy (Anderson, 2016; Richardson et al., 2006).

However, although the clinical introduction of proteasome inhibitors (PIs) has dramatically improved the overall survival of MM patients, preclinical studies using autophagy inhibitors showed contradictory results, prompting better characterization of the molecular mechanisms and substrates of autophagy in MM (Vogl et al., 2014; Milan et al., 2016; Yun et al., 2017). Autophagy is a complex recycling pathway engulfing substrates doomed to degradation in double-membrane vesicles, called autophagosomes, eventually delivered to the lysosome (Klionsky et al., 2016). Autophagy is thus capable to compensate for proteasome insufficiency by degrading poly-ubiquitinated (Ub) proteins and protein aggregates (aggrephagy) but also to clear entire organelles or portions thereof. Degradative targets are recognized by specific receptors that mediate their incorporation in the forming autophagosomes. SQSTM1/p62 is the most characterized autophagic receptor, thanks to the presence of four crucial domains: a Ub-binding activity (UBA) domain for the recruitment of poly-Ub proteins, an LC3-interacting region (LIR) bridging the substrates and the autophagosome, a Phox and Bem1 (PB1) domain for self- and hetero-polymerization, and a ZZ-type zinc finger domain (ZZ) recently proved to recognize N-terminal arginylation as a signal for autophagic proteolysis (Cha-Molstad et al., 2017; Kwon et al., 2018). In addition, p62 acts as a hub for signaling pathways, including NF-κB, mTOR, and NRF2, thereby integrating proteostasis with multiple

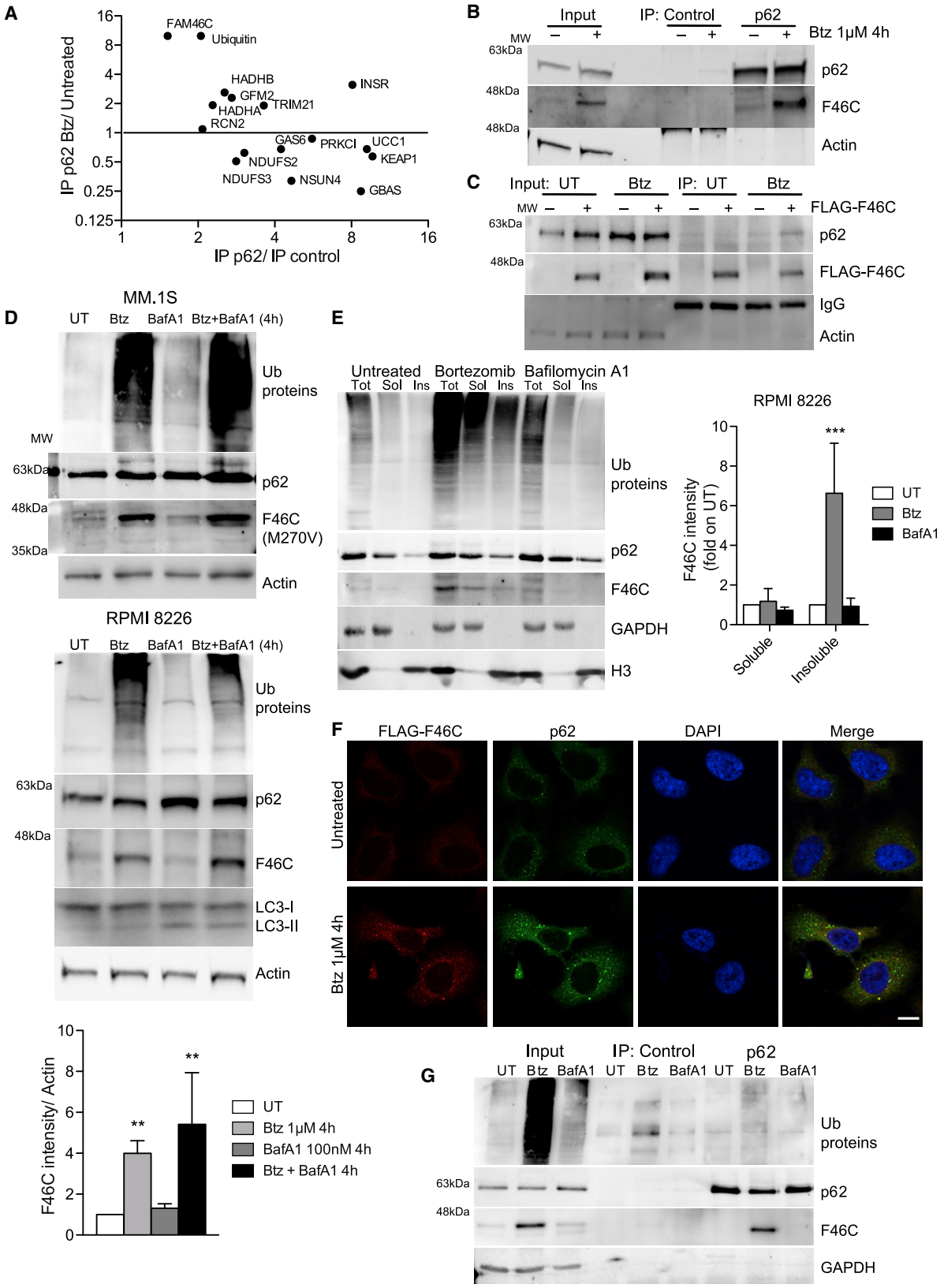

(legend on next page)

molecular functions (Moscat and Diaz-Meco, 2009; Sánchez-Martín et al., 2019). Indeed, p62-knockout (KO) mice are characterized by perturbation of metabolic processes, bone remodeling, and oxidative stress responses (Durán et al., 2004; Rodriguez et al., 2006).

In this framework, we discovered that intense constitutive autophagy is essential for normal and malignant PC survival (Milan et al., 2015; Pengo et al., 2013). Moreover, we reported that p62 is a critical mediator of the autophagic clearance of poly-Ub proteins in MM and affords specific protection against the first-in-class PI bortezomib (Milan et al., 2015). Indeed, bortezomib rapidly induces *de novo* expression of p62 and rapidly increases p62/Ub binding by ~10 times at the expense of other signaling interactors. We hypothesized that this capacity of p62 to compensate for proteasomal inhibition, granting PC survival and drug resistance, may rely on the selective degradation of specific substrates. Searching for p62 degradative targets in PCs, in the present work we discovered its interaction with FAM46C (also known as TENT5C), a protein encoded by a gene frequently and uniquely deleted in up to 20% of MM patients (Barbieri et al., 2016; Boyd et al., 2011; Chapman et al., 2011). Moreover, putative inactivating mutations of FAM46C were identified in up to 13% of patients and 25% of MM lines, implying an as yet poorly understood PC-specific tumor suppressor activity (Barbieri et al., 2016). Notably, the presence of FAM46C genetic alterations was reported to be associated with impaired overall survival of MM patients (Boyd et al., 2011).

FAM46C belongs to a metazoan-specific protein family that in humans comprises four members, annotated as non-canonical poly(A) polymerases (Kuchta et al., 2016). In line with the proposed oncosuppressive role of FAM46C, its overexpression has been reported to inhibit cell growth, to downregulate proteins that sustain MM cell survival, such as IRF4 and MYC; and to induce apoptosis in MM cell lines (Zhu et al., 2017). Independent groups showed that FAM46C polyadenylates Ig and endoplasmic reticulum (ER)-targeted mRNAs, sustains antibody responses *in vitro* and *in vivo*, and activates the unfolded protein response (UPR), suggesting a possible link with proteostasis in the secretory compartment (Bilska et al., 2020; Herrero et al., 2020; Mroczek et al., 2017). Moreover, the structure of FAM46C and its nucleotidyl-transferase catalytic site has recently been described (Chen et al., 2020). However, how FAM46C selectively harnesses the expression of ER-targeted proteins and how this function is regulated are unresolved issues. Our data disclose a potent role of FAM46C in sustaining ER biogenesis and secretory capacity through its interaction with FNDC3 proteins at the ER membrane. We also find that FAM46C activity is restrained by UPS-mediated proteolysis and by autophagy, through the inhibitory interaction with the ZZ-type domain of p62.

RESULTS

Proteasome Inhibition Induces Rapid Accumulation of the Myeloma Tumor Suppressor FAM46C and Its Aggregation with the Autophagic Receptor SQSTM1/p62

We have previously discovered that SQSTM1/p62 is essential for MM survival and affords specific protection against PI, helping the UPS cope with poly-Ub proteins (Milan et al., 2015). To characterize this compensatory role of p62 in MM cells, we defined the interactome of endogenous p62, in steady-state conditions and under treatment with the first-in-class PI bortezomib, using a SILAC (stable isotope labeling by amino acids in cell culture)-based proteomic strategy (Milan et al., 2015). Along with numerous already reported interactors (e.g., Keap1, PKCi, Ub, TRIM21, INSR), this approach revealed the association of p62 with the MM tumor suppressor FAM46C. In our dataset, FAM46C was the only protein, along with Ub, whose interaction with p62 was dramatically increased (~10 times with as little as 1 h treatment) by bortezomib (Figure 1A). We validated this interaction by immunoblot analysis after immunoprecipitation of endogenous p62 in PI-treated and control cells (Figure 1B). Of note, our proteomic analysis was performed in MM.1S cells, a FAM46C-mutated MM line. We confirmed the interaction coupling wild-type FLAG-tagged FAM46C immunoprecipitation with both unbiased liquid chromatography-tandem mass spectrometry (LC-MS/MS) analysis and immunoblotting, proving that p62/FAM46C interaction normally occurs in MM cells and is not linked to the specific M270V mutation present in MM.1S cells (Table S1; Figure 1C). Interestingly, the association, barely detectable in basal conditions, was rapidly enhanced by proteasome inhibition. However, no induction of FAM46C mRNA was detected under PI treatment, indicating that the increased interaction is not imputable to PI-induced *de novo* FAM46C expression but rather accounted for by blocked degradation (Figure S1A). Indeed, PIs (bortezomib and carfilzomib) caused rapid accumulation of both wild-type FAM46C and M270V FAM46C (in RPMI 8226 and MM.1S cells, respectively), accompanied by parallel increases of p62 and poly-Ub proteins

Figure 1. Proteasome Inhibition Induces Rapid Accumulation of FAM46C and Its Aggregation with the Autophagic Receptor SQSTM1/p62

(A) Changes of p62 interactome upon treatment with bortezomib (Btz) 1 μM for 1 h as determined by SILAC LC-MS/MS in MM.1S cells.

(B) Co-immunoprecipitation (coIP) of endogenous FAM46C (F46C) with p62 in MM.1S cells under 1 μM Btz for 4 h.

(C) Co-immunoprecipitation of p62 with FLAG-FAM46C in RPMI 8226 cells under 1 μM Btz for 4 h.

(D) Immunoblot analysis in MM cells treated with 1 μM Btz or bafilomycin A1 (BafA1) 100 nM for 4 h. Beta-actin serves as a loading control throughout. Top: representative blots; bottom: quantification of seven independent experiments (mean ± SEM; one-way ANOVA with Bonferroni post hoc test versus untreated cells; $^{**}p < 0.01$).

(E) Immunoblot analysis in Igepal CA-630 soluble and insoluble fractions of RPMI 8226 cells treated for 4 h with 1 μM Btz or 100 nM BafA1. Left: representative blots. Right: quantification of three independent experiments (mean ± SEM; two-way ANOVA with Bonferroni post hoc test; $^{***}p < 0.001$).

(F) Immunofluorescence analysis of p62 (green) and FLAG-FAM46C (red) in HeLa cells treated for 4 h with 1 μM Btz. Nuclei are stained blue with DAPI. Scale bar, 10 μm.

(G) CoIP of FAM46C with p62 in MM.1S cells under 1 μM Btz or 100 nM BafA1 for 4 h.

See also Figure S1 and Table S1.

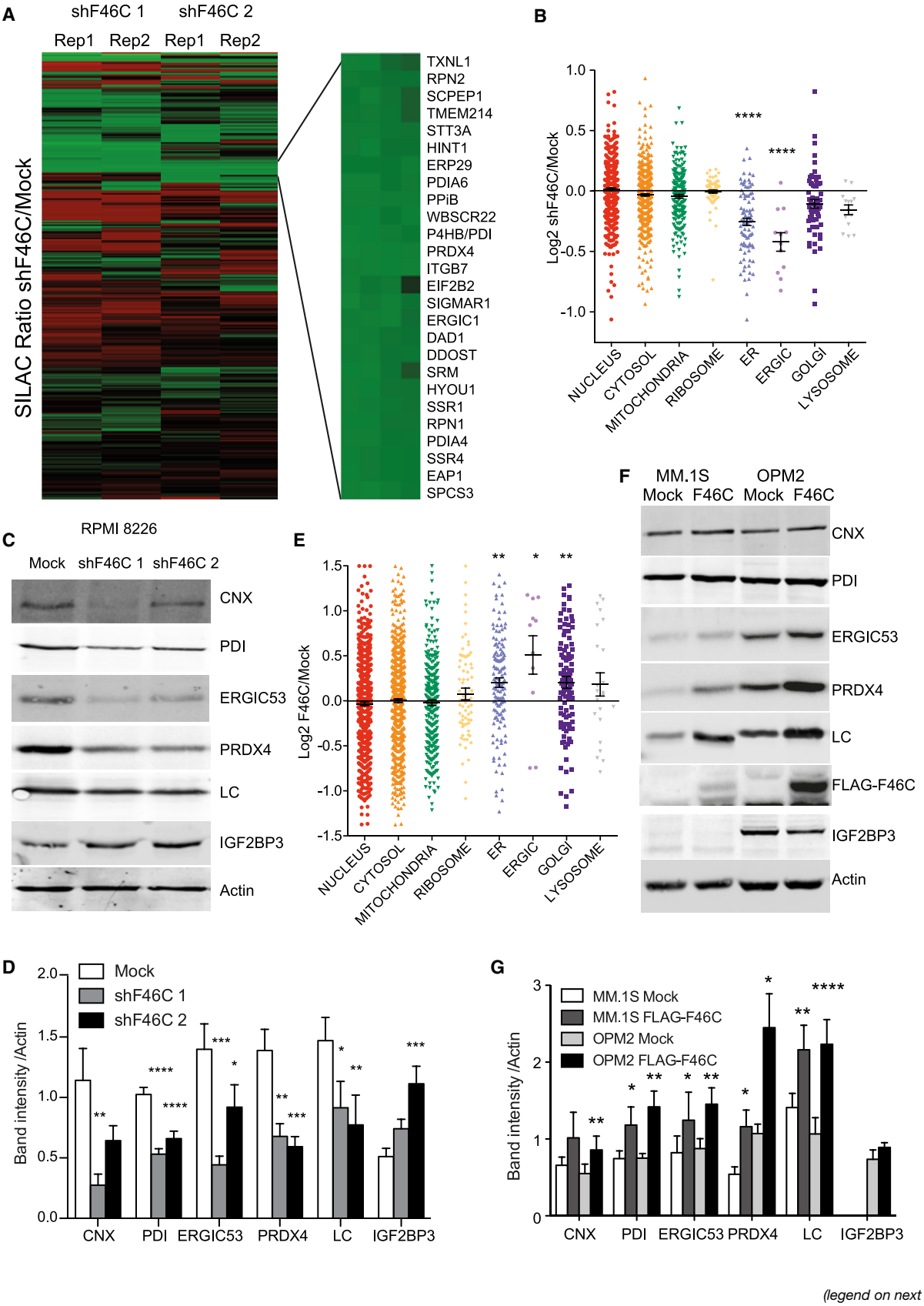

(legend on next page)

(Figure 1D; Figures S1B and S1C). Moreover, analysis of FAM46C and p62 dynamics by immunofluorescence and protein biochemistry showed that endogenous FAM46C is largely cytosolic and mild detergent soluble in untreated conditions but rapidly accumulates and colocalizes with p62 in insoluble aggregates under PIs (Figures 1E and 1F; Figures S1D and S1E). Interestingly, when the proteasome was not inhibited, distal autophagic blockade with bafilomycin A1 resulted in virtually no accumulation and aggregation in the insoluble fraction of FAM46C, proving its rapid degradation to occur mainly through the UPS (Figure 1D; Figure S1D). As a result, bortezomib, but not bafilomycin A1, rapidly (4 h) increased p62-FAM46C interaction (Figure 1G). However, the combined inhibition of autophagy and the UPS triggered additional accumulation of FAM46C, suggesting a role of autophagy and a coordinated control on FAM46C levels (Figure 1D; Figure S1F). Altogether, these data disclose that FAM46C abundance and its aggregation state are tightly and rapidly regulated by degradative pathways through the interaction with p62, implying a potentially relevant role of FAM46C in PC proteostasis.

FAM46C Upsizes the PC Secretory Apparatus and Ig Secretion

To dissect the role of FAM46C in PCs, we generated two MM lines (U266 and RPMI 8226) stably expressing two different short hairpin RNAs (shRNAs) against wild-type FAM46C, and two FAM46C-mutated MM cells (MM.1S and OPM2) in which wild-type FAM46C expression was stably restored (Figures S2A and S2B). As previously observed (Mroczek et al., 2017; Zhu et al., 2017), silenced cells showed higher clonogenic potential and proliferation rate compared with control cells (Figures S2C and S2D). Accordingly, wild-type FAM46C re-expression in mutated MM cells reduced proliferation and increased basal apoptotic rates (Figures S2E and S2F). Notably, strengthening the notion of a specific oncosuppressive role of FAM46C in PCs, its overexpression in other cell types (i.e., HeLa and HEK293T cells) did not result in proliferation defects and cell death (Figure S2G and data not shown).

To unbiasedly address the biological function of FAM46C in PCs, we performed a SILAC proteomic analysis exploiting a triple isotopic labeling to compare RPMI 8226 cells infected with a control shRNA or two different shRNAs against FAM46C. Through this approach, we identified and quantified ~1,500 proteins for each biological replicate with inverted labeling, achieving high reproducibility across the two samples (Figure 2A; Figure S2H). Statistical analysis using Perseus software was performed on 1,298 proteins quantified in both experiments with at least two peptides, identifying 147 proteins significantly modulated by the former FAM46C shRNA and 126 by the latter (Data S1; Figure 2A). Among them, the levels of 35 proteins (28 down- and 7 upregulated) were significantly and concordantly altered compared with mock cells by both shRNAs, indicating bona fide FAM46C-modulated substrates (Table S2). Briefly, silenced cells showed concerted downregulation of proteins belonging to the ER and ER-Golgi intermediate compartment (ERGIC), functionally subdivided as follows: (1) proteins mediating ER protein import (e.g., SSR1, SSR4, and SPCS3); (2) ER chaperones (MZB1 and HYOU1); (3) ER oxidoreductases and oxidative protein folding assistants (GGT2, PRDX4, and PDI family members); (4) proteins involved in ER-to-Golgi trafficking (LMAN2 and ERGIC1); (5) ER proteins involved in N-glycosylation (RPN1, DDOST, MPI, and STT3A); and (6) client secretory proteins, namely, Ig J and λ chains. DAVID Gene Ontology (GO) software showed significant enrichment of the following categories among the 28 downregulated proteins: ER lumen (GO:0005788, Benjamini adjusted $p < 0.0001$), disulfide bond (UP_Keywords, $p < 0.0001$), ER (UP_Keywords, $p = 0.015$), and glycoprotein (UP_Keywords, $p = 0.003$), while no significant GO terms were identified among upregulated proteins. Notably, among the latter category, we found the mRNA binding protein IGF2BP3 (Table S2; Figures 2C and 2D), which has been shown to promote cancer proliferation and invasiveness through the stabilization of *MYC* mRNA (Bell et al., 2013; Palanichamy et al., 2016). Next, all 1,298 quantified proteins were clustered using DAVID for their cellular compartment, revealing a crucial role of FAM46C in the homeostasis of the secretory pathway, with significant increases of ER and ERGIC protein levels (Figure 2B). Our proteomic data were validated by immunoblot analysis of selected ER and ERGIC proteins in silenced RPMI 8226 and U266 cells (Figures 2C and 2D; Figure S2I). Moreover, attesting to functional relevance, the decrease of proteins involved in the secretory apparatus was coupled with downregulation of both intracellular and secreted Ig light chain (LC) (Figure S3A).

In line with the results obtained in silenced cells, wild-type FAM46C re-expression in mutated MM lines significantly increased the levels of ER, ERGIC, and Golgi proteins and Igs, as assessed by label-free proteomics and immunoblot analysis (Data S2; Figures 2E–2G). Accordingly, FAM46C-mediated ER expansion resulted in increased LC secretion by OPM2 cells (Figure S3B), whereas no clear effects of FAM46C re-expression

Figure 2. FAM46C Silencing Reduces ER Protein Levels in MM Cells

(A) Heatmap of SILAC ratios for 1,298 proteins quantified in both experiments in RPMI 8226 cells (green, downregulated; red, upregulated by FAM46C silencing).

(B) Quantified proteins were grouped by GO categories (average ratios ± SEM; one-way ANOVA with Bonferroni post hoc test versus all the quantified proteins, *$p < 0.05$, ****$p < 0.0001$).

(C) Immunoblot analysis in FAM46C-silenced RPMI 8226 cells.

(D) Quantification of band intensities of at least six independent experiments represented in (C) (mean ± SEM; repeated-measures one-way ANOVA with Bonferroni post hoc test versus mock cells, *$p < 0.05$, **$p < 0.01$, ***$p < 0.001$, ****$p < 0.0001$).

(E) Proteome changes in FAM46C-overexpressing OPM2 cells by label-free LC-MS/MS analysis. The 1,688 proteins quantified in both replicates were grouped by GO categories (average ratios ± SEM; one-way ANOVA with Bonferroni post hoc test versus all the quantified proteins, *$p < 0.05$, **$p < 0.01$).

(F) Immunoblot analysis in FAM46C-overexpressing OPM2 and MM.1S cells.

(G) Quantification of band intensities of at least six independent experiments represented in (F) (mean ± SEM; paired t test FAM46C versus mock cells, *$p < 0.05$, **$p < 0.01$, ****$p < 0.0001$).

See also Figure S2, Table S2, and Data S1 and S2.

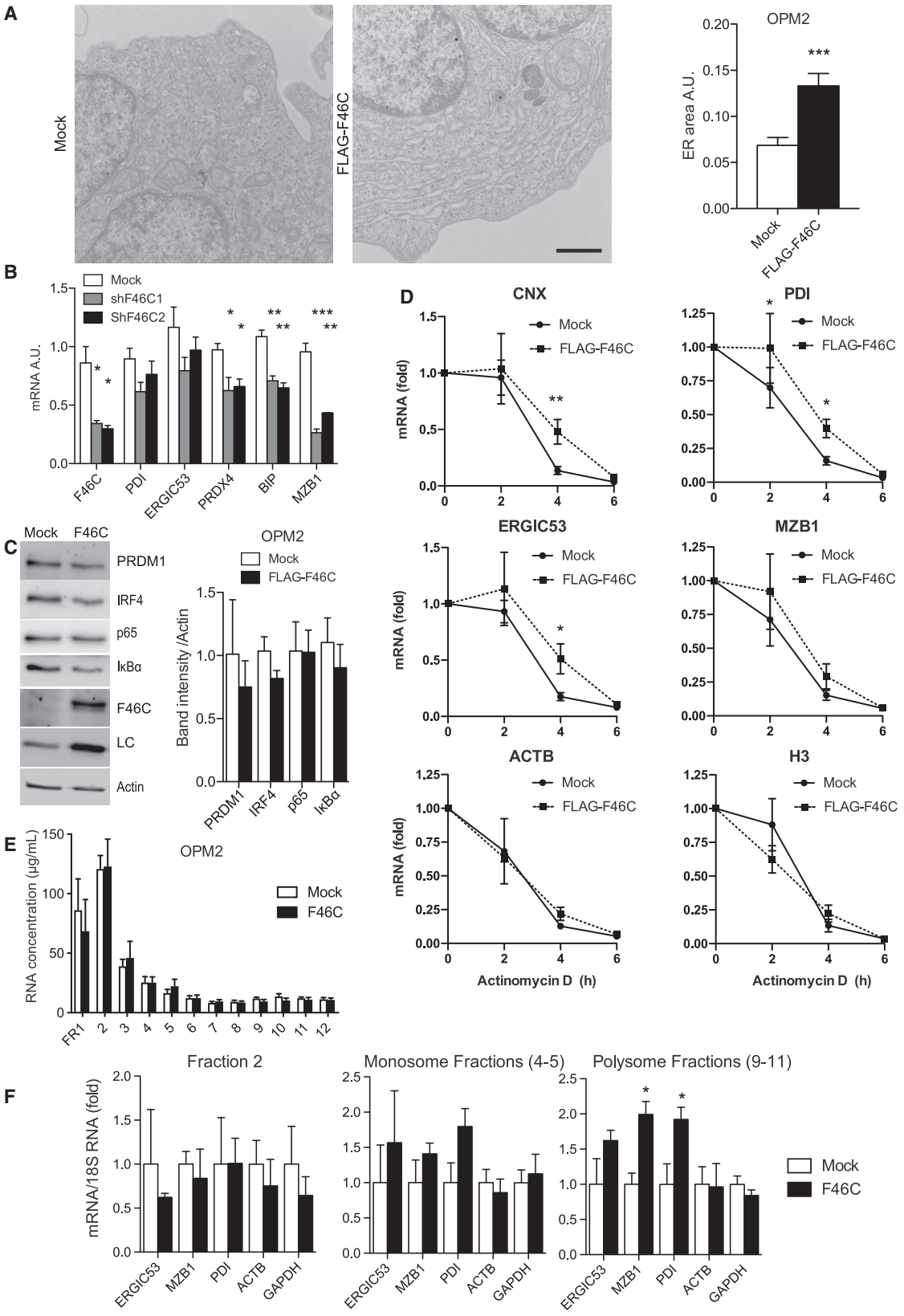

(legend on next page)

were noted on IGF2BP3, suggesting the lack of a direct mechanistic link between the two proteins (Figures 2F and 2G). Electron microscopy analysis revealed that wild-type FAM46C re-expression also has dramatic effects on ER morphology, almost doubling ER area with the appearance of dilated cisternae (Figure 3A). In line with the poly(A) polymerase activity of FAM46C, we found a corresponding modulation in the abundance of transcripts encoding ER-targeted proteins in both FAM46C-silenced and overexpressing cells (Figure 3B; Figure S3C), while no significant effects at the mRNA and protein levels were observed on PC identity factors (e.g., PRDM1, IRF4, XBP1, NF-κB) known to sustain ER expansion during PC differentiation (Figure 3C; Figures S3D–S3F), with the possible exception of IRF4, which we found to decrease, albeit non-significantly, upon FAM46C expression, as previously reported (Zhu et al., 2017). Indicative of an ER-selective mRNA-stabilizing activity of FAM46C, transcripts encoding ER and ERGIC proteins showed increased stability in FAM46C-expressing cells, while that of transcripts lacking poly(A) or encoding a cytosolic protein, namely, H3 and beta-actin mRNAs, was unchanged (Figure 3D). Finally, we assessed the effect of FAM46C expression on mRNA portioning in polysomes. FAM46C had no effect on total mRNA abundance in different sucrose fractions (Figure 3E; Figure S3G) but induced a significant enrichment of ER-targeted transcripts in the polysome-containing fractions (Figure 3F).

Altogether, our unbiased approaches identified a potent and direct role of the MM tumor suppressor FAM46C in sustaining ER expansion and antibody secretion in PCs through a selective positive control of ER protein translation.

Expression of FAM46C and FAM46D Exaggerates ER Capacity and Ig Secretion beyond Sustainability

Notably, FAM46C is a member of a metazoan-specific protein family that comprises four members sharing ~50% sequence identity, but mutations were identified only in FAM46C. To explore FAM46C specificity, we overexpressed all four family members in FAM46C-mutated MM cells. Interestingly, FAM46C and testis-specific FAM46D had drastic effects on the expression of ER proteins and ER size, while FAM46A and FAM46B had, respectively, intermediate and no effects (Figures 4A and 4B; Figure S4A). Relevant to MM pathobiology, the ER-expanding and cytotoxic effects of FAM46 proteins coincided, as FAM46C and FAM46D expression triggered MM cell death and rapid counter-selection for low expressing cells, whereas FAM46A and FAM46B were well tolerated (Figures 4C; Figure S4B). Sustained Ig production implies high energy expenditure for protein synthesis, folding, and trafficking and remarkable oxidative stress (Cenci et al., 2011). Accordingly, FAM46C and FAM46D expression significantly reduced intracellular ATP levels (Figure 4D; Figure S4C) and induced reactive oxygen species (ROS) accumulation (Figure 4E).

Interestingly, by comparing proteasome-mediated degradation of FAM46 members, we found that protein stability inversely correlated with the capacity to induce ER expansion. Indeed, FAM46A and FAM46B appeared significantly less degraded by the UPS than FAM46C and FAM46D in both MM and HEK293T cells (Figure 4F; Figures S4D and S4E). These data suggest the possibility that ER-expanding FAM46 proteins require a tighter degradative control to afford a sustainable equilibrium between protein secretion and cellular stress.

Overall, our findings disclose a role of FAM46C in boosting ER biogenesis, secretory capacity, and Ig secretion beyond sustainability. The data may explain the selective pressure in MM cells to inactivate FAM46C so as to reduce secretory protein load and ER stress in favor of proliferation and survival.

FAM46C is Induced by PRDM1 in MM Cells and Interacts with FNDC3 Proteins on the ER Membrane

Then, we challenged the cell type specificity of the identified functional effects of FAM46 proteins. To do so, we forced their expression in non-PCs as wild-type HeLa and HEK293T cells stably expressing human uromodulin as a paradigmatic client secretory protein (Schaeffer et al., 2009) under a UPR- and PC-unrelated constitutive promoter (CMV). Interestingly, similar to PCs, FAM46C and FAM46D increased ER size in both cell types and uromodulin secretion in HEK293T cells, indicating that the underlying molecular mechanism is independent of cell type and of the promoter driving ER-targeted proteins (Figure 5A; Figure S5A). Having found that the positive secretory effect of FAM46C is in principle not restricted to PCs, while its mutations are MM specific, we hypothesized that FAM46C is expressed mainly in PC ontogeny. In keeping with this hypothesis, FAM46C is distinctively expressed in lymphoid tissues and testis in humans (Uhlén et al., 2015; www.proteinatlas.org). Moreover, PCs are the highest FAM46C-expressing cells among all cancer lines (Ghandi et al., 2019; https://www.depmap.org/). We then checked its expression in differentiating PCs. As previously demonstrated in other studies (Bilska et al., 2020; Mroczek et al., 2017), using murine LPS-activated splenic B lymphocytes, we found that FAM46C is strongly induced during PC

Figure 3. FAM46C Expression Sustains ER Expansion and Ig Secretion in MM Cells

(A) Electron microscopy analysis of FAM46C-overexpressing and mock OPM2 cells. Left: representative images (scale bar: 1 μm); right: quantification by stereology of the area occupied by the ER (mean ± SEM; n = 20 cells per line; Welch's t test, ***p < 0.001).

(B) qRT-PCR analysis in FAM46C-silenced U266 cells (mean ± SEM normalized on H3 mRNA; n = 3; one-way ANOVA with Bonferroni post hoc test versus mock cells, *p < 0.05, **p < 0.01, ***p < 0.001).

(C) Immunoblot analysis in FAM46C-overexpressing OPM2 cells. Left: representative blots; right: quantification of band intensities (mean ± SEM; n = 3).

(D) qRT-PCR analysis in FAM46C-overexpressing OPM2 cells treated for the indicated time with actinomycin D (mean ± SEM normalized on 18S RNA; n = 4; repeated-measures two-way ANOVA with Bonferroni post hoc test, *p < 0.05, **p < 0.01).

(E) Quantification of absorbance at 260 nm in density fractions obtained by ultracentrifugation of OPM2 cell lysates (mean ± SEM; n = 5).

(F) qRT-PCR analysis in the indicated sucrose fractions from FAM46C-overexpressing and control OPM2 cells (mean ± SEM normalized on 18S RNA; n = 3; paired t test, FAM46C versus mock cells, *p < 0.05).

See also Figure S3.

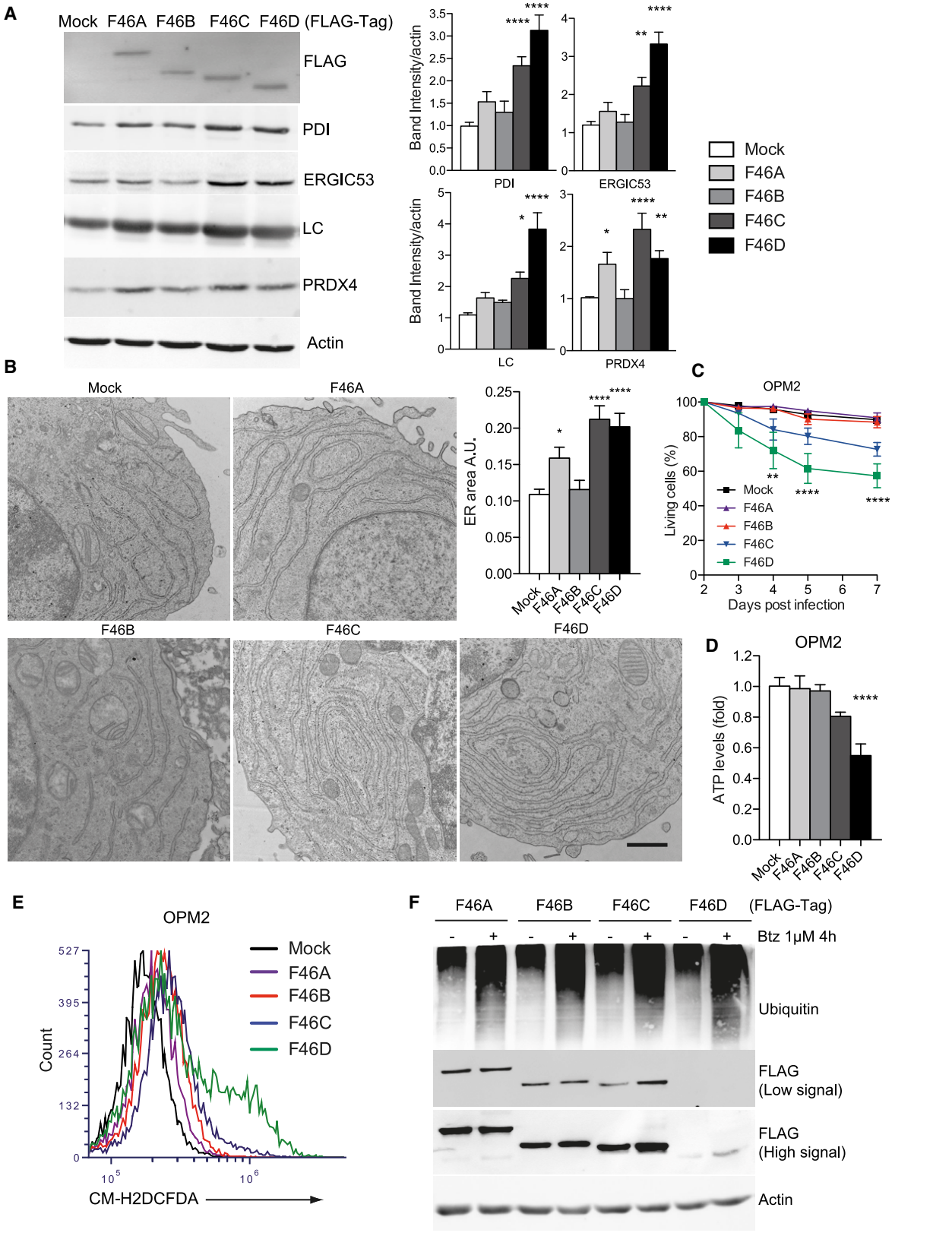

(legend on next page)

differentiation (Figures S5B and S5C). In line with this, published datasets from two independent groups revealed FAM46C as a direct target of the master PC transcriptional regulator PRDM1 by RNA sequencing (RNA-seq) and chromatin immunoprecipitation sequencing (ChIP-seq) experiments in primary PCs (Minnich et al., 2016; Tellier et al., 2016). Accordingly, PRDM1 silencing significantly reduced FAM46C mRNA and protein levels in human MM cells (Figures 5B and 5C; Figure S5D). Together with the ER-biogenetic capacity disclosed above, these findings define a mechanism contributing to ER development in PCs. The selective effects of FAM46C on the ER have been proposed to rely on its partial ER localization (Bilska et al., 2020). Indeed, by immunofluorescence, we documented that FAM46C partially colocalized with the ER marker calnexin in both MM and HeLa cells (Figure 5D; Figure S5E). To disclose the molecular partner involved in its ER localization and gauge its role in the selective regulation of FAM46C on ER-targeted transcripts, we defined the interactome of FAM46C in MM cells overexpressing FLAG-FAM46C. LC-MS/MS analysis of co-immunoprecipitated proteins identified, along with p62, few putative specific interactors of FAM46C suggesting a quite selective molecular action in PCs. In particular, we identified the poly(A)-binding proteins PABPC1 and PABPC4, in line with the proposed role in mRNA stability, and the interaction with FNDC3B (Table S1). Of note, FNDC3B is an ER transmembrane protein with a single transmembrane domain at the C terminus preceded by nine repeated fibronectin type III domains facing the cytosol, whose molecular function is unknown. Interestingly, like FAM46C, FNDC3B is part of a protein family, with a paralog, FNDC3A, sharing 50% amino acid sequence. We documented the interaction of FAM46C with both FNDC3B and FNDC3A by immunoprecipitation of FLAG-FAM46C or endogenous FNDC3B (Figure 5E; Figure S5F). Moreover, we confirmed their colocalization by immunofluorescence in HeLa and MM cells (Figure 5F; Figure S5G). Corroborating a mechanistic link between ER biogenesis and association with FNDC3 proteins (Figure 5E), ER-expanding activity, binding with FNDC3 proteins and presence in the membrane-associated fraction overtly correlated across FAM46 family members (Figure 5G; Figure S5H).

FAM46C Interaction with FNDC3 Proteins at the ER Membrane Is Essential for ER Expansion

To gauge the role of the interaction of FAM46C with FNDC3 proteins in its selectivity for ER-targeted mRNAs, we generated FNDC3-silenced MM cells. Consistently with FAM46C effects, FNDC3B silencing decreased ER protein content and Ig levels (Figure 6A), while FNDC3A silencing had lower effects (Figure S6A). Surprisingly, FNDC3B caused a reduction of ER protein levels also in FAM46C-mutated OPM2 cells (Figure 6A), suggesting that FNDC3B may be essential for proper ER homeostasis independently of FAM46C or that the FAM46C mutation present in OPM2 cells (E178A) does not fully abrogate FAM46C activity. To gauge the role of FAM46C/FNDC3B interaction, we overexpressed FAM46C in FNDC3B-silenced cells and found that FAM46C maintained the ability to increase the abundance of ER proteins (Figure S6B), indicating a possible compensation by FNDC3A consistent with their substantial sequence identity. We thus generated double-knockdown RPMI 8226 and OPM2 cells (Figure S6C). Consistent with a key role of FNDC3 proteins in FAM46C stabilizing activity, double-knockdown cells showed reduced mRNA stability of ER and ERGIC-targeted transcripts (Figure 6B). Silencing both FNDC3 proteins also resulted in complete toxicity compared with single silencing 7 days post-lentiviral infection (data not shown). However, the overexpression of FAM46C before the onset of toxicity upon double FNDC3 knockdown failed to increase ER mRNAs and proteins in MM cells (Figures 6C and 6D; Figures S6D and S6E), proving that the capability of FAM46C to upsize the ER requires at least one FNDC3 protein. Finally, FNDC3 double knockdown substantially reduced the amount of FAM46C in the membrane fraction (Figure 6E), proving FAM46C localization at the ER membrane dependent on FNDC3 proteins.

Under Proteostatic Stress, p62 Diverts Excess FAM46C from FNDC3 Proteins through Its ZZ-Type Domain

Among FAM46C interactors in our proteomic analysis, along with FNDC3B we confirmed its binding to p62 (Table S1). However, we never identified FNDC3 proteins in our repeated p62 immunoprecipitations, nor did we detect p62 in FNDC3B immunoprecipitates, suggesting that p62, FAM46C, and FNDC3 proteins are not present in the same complex. Moreover, immunoprecipitation experiments in bortezomib-treated cells showed that the accumulation of FAM46C caused by UPS inhibition does not increase its binding with FNDC3 proteins, but only with the autophagic receptor p62 (Figure 7A). Moreover, we found that upon PI treatment, FAM46C rapidly became insoluble and aggregated with p62 (Figures 1E and 1F). Immunofluorescence analyses in MM cells showed that these FAM46C-p62-positive aggregates

Figure 4. Expression of FAM46C and FAM46D Increases ER Capacity and Ig Secretion beyond Sustainability

(A) Immunoblot analysis in OPM2 cells expressing FAM46 family members. Left: representative blots; right: quantification of band intensities (mean ± SEM; n ≥ 3; repeated-measures one-way ANOVA with Bonferroni post hoc test versus mock cells, *p < 0.05, **p < 0.01, ****p < 0.0001).

(B) Electron microscopy analysis in MM.1S cells overexpressing FAM46 family members. Left: representative images (scale bar, 1 μm); right: quantification by stereology of the area occupied by the ER (mean ± SEM; n = 20 cells per line; one-way ANOVA with Bonferroni post hoc test versus mock cells, *p < 0.05, ****p < 0.0001).

(C) Equal numbers of OPM2 cells were seeded and counted for 6 days after trypan blue staining (n = 3; two-way ANOVA with Bonferroni post hoc test versus mock cells, **p < 0.01, ****p < 0.0001).

(D) Intracellular ATP measured in OPM2 cells overexpressing FAM46 proteins at day 3 post-infection (mean ± SEM; n = 4; one-way ANOVA with Bonferroni post hoc test versus mock cells, ****p < 0.0001).

(E) Cytofluorimetric assessment of ROS content upon CM-H2DCFDA staining in OPM2 cells overexpressing FAM46 proteins.

(F) Immunoblot analysis in OPM2 cells expressing FLAG-FAM46 members treated with bortezomib 1 μM for 4 h. See Figure S4D for band quantifications.

See also Figure S4.

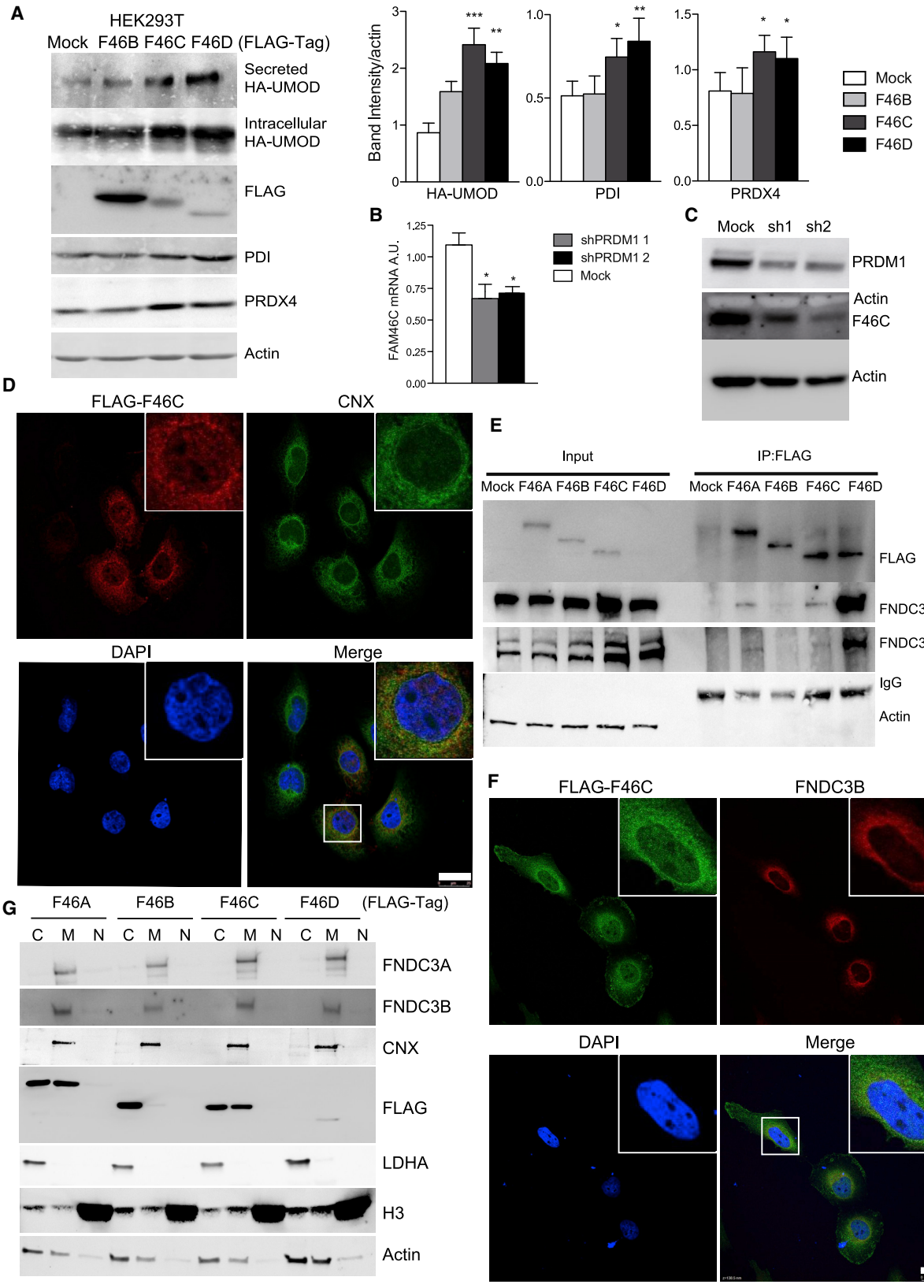

(legend on next page)

are not localized at the ER membrane (Figure 7B). Taken together, these results suggest that under perturbed proteostasis, p62 may act as a sponge for surplus FAM46C, restricting its binding to FNDC3 proteins.

Several proteins, such as DAXX and NBR1, have been shown to interact with p62, inducing its phosphorylation and phase separation in liquid bodies and mediating Nrf2 activation (Sánchez-Martín et al., 2020; Yang et al., 2019). However, FAM46C overexpression had no impact on p62 phosphorylation at S349 and S403 residues and Nrf2 target gene expression in both untreated and bortezomib-treated conditions (Figures S7A–S7C).

We then sought to address the role and molecular requirements of p62 association with FAM46C. First, we found that p62 overexpression was not sufficient to cause FAM46C accumulation in the insoluble fraction or to increase its sequestration in untreated conditions, suggesting that increased binding of FAM46C with p62 aggregates is linked with UPS impairment (Figures S7C and S7D). Notably, we previously reported that p62 is vital in MM cells, as p62-silenced MM cells underwent complete extinction in less than 1 week (Milan et al., 2015). Cell death was preceded by reduced PRDM1 and FAM46C mRNA expression, hampering the study of FAM46C dynamics in MM cells (Figure S7E). We thus exploited CRISPR technology to generate HeLa p62-KO cells expressing FLAG-FAM46 proteins found to upsize the ER (Figure S7F). Notably, FAM46C and FAM46D expression exerted no overt toxicity in p62 WT HeLa cells, while they induced cell death (Figure 7C) and rapid selection for low-expressing cells (not shown) in the absence of p62, unveiling a fundamental role of p62 in preventing FAM46-induced toxicity. Moreover, confirming our hypothesis of p62 buffering excess FAM46C, in p62-KO cells the interaction of FAM46C with FNDC3 proteins was increased relative to its low abundance (Figure 7D). We then addressed which motif of p62 is required for its interaction with FAM46C by reconstituting HeLa p62-KO cells with p62 mutants lacking the principal domains (i.e., PB1, ZZ, LIR, KIR, and UBA). Immunoprecipitation experiments showed that FAM46C interaction is mediated by the ZZ domain and not by the UBA or other moieties (representative data for UBA and ZZ domains in Figure 7E and Figure S7G). However, we were unable to identify any Ub-FAM46C peptide or other post-translation modification among those sequenced in our immunoprecipitation MS analysis (Table S1; Data S3). Accordingly, the p62-ZZ domain inhibitor XRK3F2 reduced PI-induced p62/FAM46C interaction (Figure 7F). To gauge the protective role of p62 ZZ domain in coping with PI-driven FAM46C accumulation, we treated FAM46C-wild-type RPMI 8226 cells with subtoxic doses of bortezomib and XRK3F2, alone and in combination. Combined PI and XRK3F2 treatment resulted in accumulation of FAM46C and Ub proteins (Figure 7G) and slightly synergic cell death (Figure 7H) as assessed by the Chou-Talalay combination index (Figure S7H).

These findings reveal a key protective function of p62 under proteostatic stress, through FAM46C sequestration via its ZZ domain, preventing excessive ER expansion and related toxicity.

DISCUSSION

Upon antigen stimulation, B cells undergo profound proteome reshaping to become antibody factories, through the concerted increase of the size and capacity of their secretory apparatus (Brewer and Hendershot, 2005; Sitia and Braakman, 2003). This differentiation process is ensured by a genetic reprogramming involving master transcription factors such as IRF4, PRDM1, and XBP-1 (Nutt et al., 2011, 2015; Turner et al., 1994). In particular, PRDM1 acts not only as a key repressor of B cell identity factors such as BCL6 and PAX5 but also as a transcriptional activator promoting Ig and XBP-1 expression and the conversion of Ig heavy chains to the secreted form (Martins and Calame, 2008; Minnich et al., 2016; Tellier et al., 2016). Interestingly, XBP-1 overexpression in PRDM1-deficient cells is not able to restore normal Ig production, suggesting that PRDM1 functions extend beyond the induction of the Ire-1 branch of the UPR (Shapiro-Shelef et al., 2003, 2005). In the present work, we disclosed a mechanism involving the MM-specific tumor suppressor FAM46C contributing to shape the distinctive PC secretory capacity under PRDM1 (Figure 5). Indeed, we found that FAM46C expression is sufficient to promote the rapid and concerted expression of ER and ERGIC proteins and Igs, potently enhancing the secretory capacity of MM cells (Figures 2 and 3). Of note, FAM46C has been shown to be a non-canonical poly(A) polymerase that preferentially polyadenylates and stabilizes ER-targeted transcripts (Bilska et al., 2020; Herrero et al., 2020; Mroczek et al., 2017), through an as yet undefined mechanism. Our unbiased identification of the poly(A)-binding proteins PABPC1 and PABPC4 in the FAM46C interactome (Table S1) is in line with the proposed enzymatic activity, as are our

Figure 5. FAM46C Is Induced by PRDM1 in MM Cells and Interacts with FNDC3 Proteins at the ER Membrane

(A) Immunoblot analysis in HEK293T cells expressing FAM46 family members and secreting HA-tagged human uromodulin (HA-UMOD). Left: representative blots; right: quantification of band intensities (mean ± SEM; n = 6; repeated-measures one-way ANOVA with Bonferroni post hoc test versus mock cells, $^{*}p < 0.05$, $^{**}p < 0.01$, $^{***}p < 0.001$).

(B) qRT-PCR analysis of FAM46C mRNA levels in PRDM1 silenced RPMI 8226 cells (mean ± SEM normalized on H3 mRNA; n = 4; one-way ANOVA with Bonferroni post hoc test versus mock infected cells, $^{*}p < 0.05$).

(C) Immunoblot analysis in PRDM1 silenced RPMI 8226 cells.

(D) Immunofluorescence analysis of calnexin (green) and FLAG-FAM46C (red) in HeLa cells. Nuclei are stained blue with DAPI. White insets show detail magnification. Scale bar, 25 μm.

(E) Co-immunoprecipitation of FNDC3 proteins with FLAG-FAM46 proteins in OPM2 cells. Samples were loaded on a nUView 8%–16% Tris-Glycine Gel (NuSep, NB12-816), in which migration pattern of FAM46 proteins differs from homemade gels used in the other panels.

(F) Immunofluorescence analysis of FLAG-FAM46C (green) and FNDC3B (red) in HeLa cells. Nuclei are stained blue with DAPI. White insets show detail magnification. Scale bar, 25 μm.

(G) Immunoblot analysis in different cellular fractions. Quantifications are reported in Figure S5H.

See also Figure S5 and Table S1.

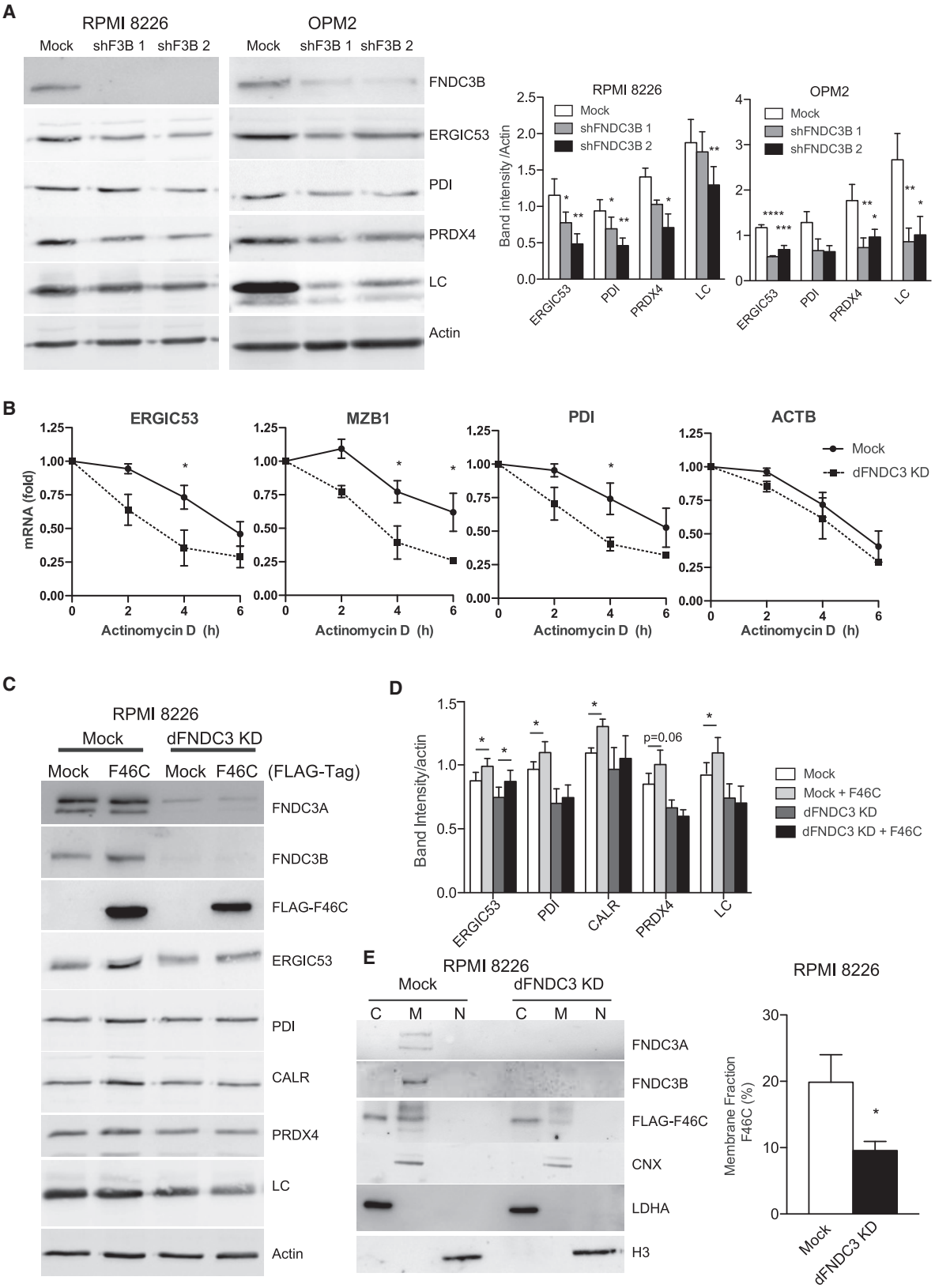

(legend on next page)

data reporting (1) selective stabilization of transcripts encoding ER and ERGIC proteins (Figure 3), (2) a consistent effect of FAM46C up- or down-modulation on ER-targeted mRNA and protein levels (Figures 2 and 3), and (3) significant enrichment of ER transcripts in polysome-containing fractions (Figure 3). As a result, FAM46C has a major impact on the secretory capacity through enhanced ER-associated translation and import of proteins mediating oxidative folding, N-glycosylation, and trafficking along the secretory route.

The specificity of FAM46C activity on ER-targeted transcripts remained unexplained except for a recently proposed localization of FAM46C to the ER membrane (Bilska et al., 2020). Our data show that FAM46C activity depends on its localization at the ER membrane in a complex with FNDC3A and FNDC3B, two high-molecular weight proteins sharing 50% sequence identity, whose molecular functions were still virtually unknown. In particular, FNDC3B expression has been shown to correlate with UPR induction and poor prognosis in cervical cancer (Han et al., 2020); however, its oncogenic role is still unclear, as it has been shown both to inhibit and to promote cell invasiveness in different solid cancers (Fan et al., 2013; Lin et al., 2016; Yang et al., 2017). We identified FNDC3B in an unbiased proteomic analysis of the FAM46C interactome. Moreover, we demonstrated FAM46C interaction also with the paralog FNDC3A by immunoblot analysis (Table S1). Notably, in our hands, FAM46C was able to exert its ER-expanding activity in single-FNDC3-silenced cells, whereas it lost it upon double FNDC3 silencing, indicating functional redundancy of the two proteins (Figure 6). Moreover, we observed that the combined knockdown of FNDC3 proteins was toxic for MM cells, indicating that FNDC3 proteins have at least one FAM46C-independent role essential for MM survival.

Of interest, also FAM46C is part of a family with four members, all predicted *in silico* to be non-canonical poly(A) polymerases (Kuchta et al., 2016). However, testing their overexpression, we found that they drastically differ for FNDC3 binding, ER effects, and PC toxicity. In particular, we disclosed that FAM46D is the most effective and toxic member of the family, while FAM46B has lesser effects on the ER (Figures 4 and S4). However, FAM46D is not expressed in PCs, as it is a testis-specific protein of unknown function (Uhlén et al., 2015; www.proteinatlas.org), hinting at a potential role of the FAM46/FNDC3 axis in spermatogenesis. Strengthening this hypothesis, both FAM46C and FNDC3A-KO mice resulted in male sterility, characterized by the presence of abnormal spermatozoa (Obholz et al., 2006; Zheng et al., 2019). Similarly, the biological function of the other two members is still elusive, although FAM46A seems to have a role in bone biology (Diener et al., 2016; Doyard et al., 2018), while FAM46B has been recently reported to block prostate cancer cell proliferation through the inhibition of β-catenin signaling (Liang et al., 2018). Relevant for MM biology, we found that the differential impact of FAM46 proteins on secretory activity strongly correlated with their toxicity, offering a plausible mechanistic explanation. Indeed, intense Ig production implies significant expenditure of intracellular ATP for protein synthesis, folding, and trafficking (Sitia and Braakman, 2003). Moreover, the formation of a large number of disulfide bonds crucial for proper Ig folding generates remarkable oxidative stress in PCs (Gross et al., 2006; Shimizu and Hendershot, 2009). Accordingly, we showed that FAM46C- and FAM46D-mediated increase in the secretory activity induces ROS accumulation, ATP decrease, and cell death (Figure 4). On the contrary, FAM46C-silenced cells showed higher proliferation and clonogenic potential (Figure S2). Altogether, our data provide a role of FAM46C in ER biogenesis and secretory homeostasis. This role is likely to explain the selective advantage for MM cells inactivating FAM46C to decrease ER stress and Ig production in favor of energy balance and proliferation. In keeping with this interpretation, deletions and truncating mutations in *PRDM1* and *XBP1* have also been identified in MM patients (Bolli et al., 2018; Hoang et al., 2018; Kortüm et al., 2015). Notably, our discovery of a FAM46C/FNDC3 protein axis potentially capable to rapidly and potently harness the folding and secretory capacity in all cells (Figure 5) opens the possibility to exploit FAM46-related strategies to maximize antibody production for biotechnological and therapeutic purposes or to alleviate genetic ER-folding diseases.

Finally, the proteosynthetic activity required for humoral immunity leads to the abundant production of rapidly degraded polypeptides (RDPs) and ER misfolded by-products (Cenci et al., 2012; Haynes et al., 2004; Schubert et al., 2000). The resulting protein overload generates a delicate balance between Ig synthesis and degradative capacity, considered a peculiar "Achilles' heel" typical of PCs, of great therapeutic value (Cenci, 2012). How PCs maintain this equilibrium is a critical aspect for their survival and a goldmine for current and future therapeutic opportunities. Hence, the identification and characterization of specific molecular factors regulating PC proteostatic burden, like the p62/FAM46C/FNDC3 axis, may disclose therapeutic targets against MM.

Of note, we discovered that FAM46C levels and activity are tightly regulated by protein degradation in a manner that involves an interplay of the UPS and the autophagic receptor p62. Indeed, FAM46C is constantly degraded by the UPS but rapidly interacts

Figure 6. FAM46C Interaction with FNDC3 Proteins at the ER Membrane Is Essential for ER Expansion

(A) Immunoblot analysis in FNDC3B-silenced RPMI 8226 and OPM2 cells. Left: representative blots; right: quantification of band intensities (mean ± SEM; n = 4; repeated-measures one-way ANOVA with Bonferroni post hoc test versus mock infected cells, *p < 0.05, **p < 0.01, ***p < 0.001, ****p < 0.0001).

(B) qRT-PCR analysis in FNDC3 double-knockdown RPMI 8226 cells treated for the indicated time with 10 μg/mL actinomycin D (mean ± SEM normalized on 18S RNA; n = 3; repeated-measures two-way ANOVA with Bonferroni post hoc test, *p < 0.05).

(C) Immunoblot analysis in FNDC3 double-knockdown RPMI 8226 cells. Cells were infected with shRNAs against FNDC3 mRNAs. After 48 h lentivirus encoding FLAG-FAM46C cDNA was added, and lysates were collected 3 days after the second infection.

(D) Quantification of band intensities of six experiments represented in (C) (mean ± SEM; paired t test FAM46C versus mock infected cells, *p < 0.05).

(E) Immunoblot analysis for FAM46C cellular distribution in FNDC3 double-knockdown RPMI 8226 cells. Left: representative blot; right: quantification of FAM46C abundance in the membrane-associated fraction (mean ± SEM; paired t test FAM46C versus mock cells, *p < 0.05).

See also Figure S6.

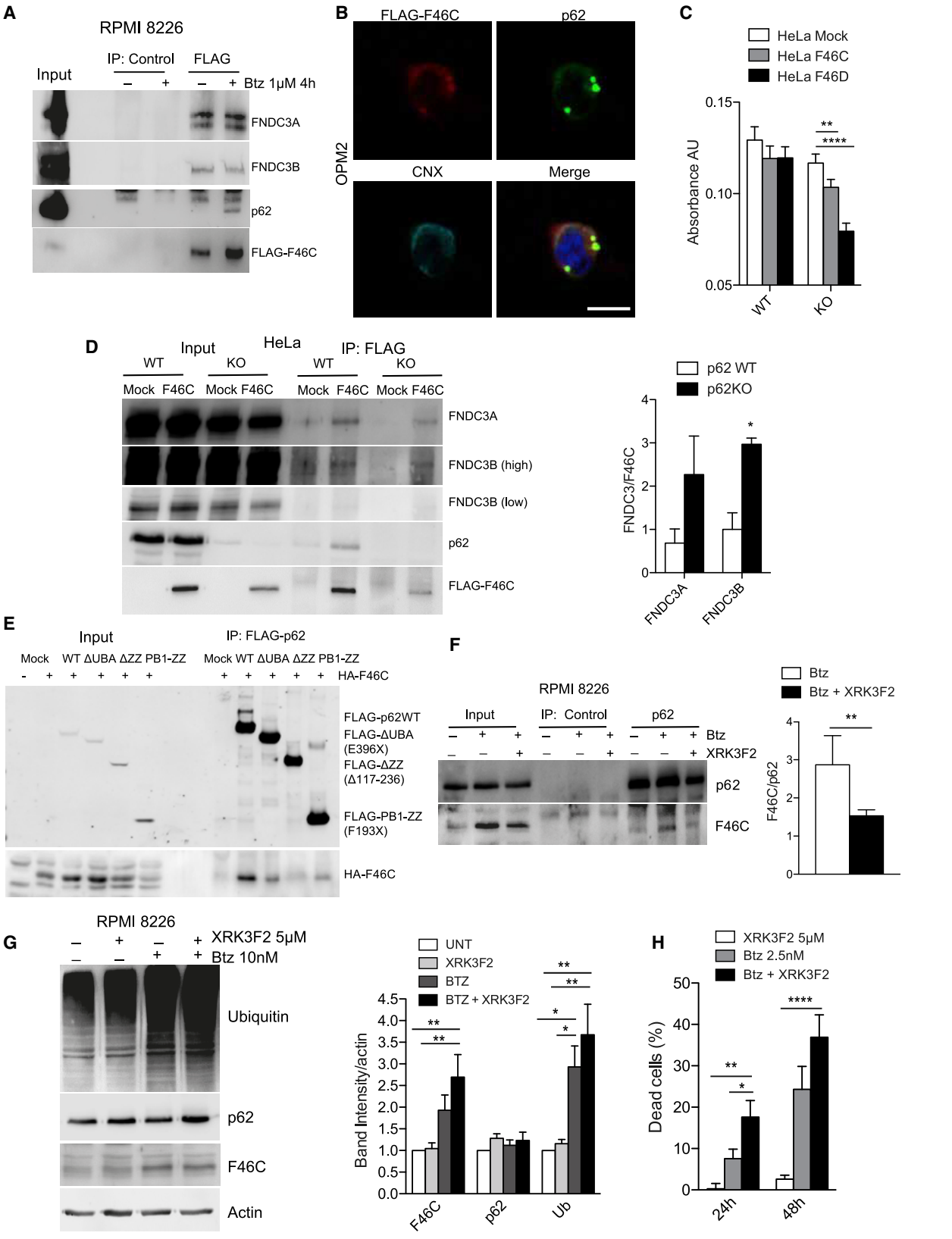

(legend on next page)

with the ZZ domain of p62 when proteasomal degradation is impaired (Figures 1 and 7). Thus, p62 acts as a buffer, aggregating with FAM46C and preventing its interaction with FNDC3 proteins. Attesting to a vital role of p62-dependent FAM46C control, we found that the absence of p62 is sufficient to trigger FAM46C toxicity in HeLa cells. To challenge this protective role of p62 dampening FAM46C activity in PI-treated cells, we exploited the specific ZZ domain inhibitor XRK3F2. Of note, XRK3F2 was already shown to inhibit MM growth *in vitro* and *in vivo*, indicating a therapeutic potential against MM (Teramachi et al., 2016). We showed that in PI-treated MM cells, XRK3F2 treatment blunted p62/FAM46C association, induced accumulation of FAM46C and Ub proteins, and increased the toxicity of bortezomib (Figure 7).

Taken together, we discovered a p62/FAM46C/FNDC3 molecular interplay integrating ER secretory capacity and degradative pathways, which is essential for PCs to maintain a sustainable equilibrium between Ig production and proteosynthetic stress. This circuit offers an array of potential therapeutic strategies that could be exploited to achieve selective cancer cell death and to increase PI efficacy against MM.

STAR★METHODS

Detailed methods are provided in the online version of this paper and include the following:

- KEY RESOURCES TABLE
- RESOURCE AVAILABILITY
  - Lead Contact
  - Materials Availability
  - Data and Code Availability
- EXPERIMENTAL MODEL AND SUBJECT DETAILS
  - Cell lines
  - Animal models
- METHOD DETAILS
  - Proliferation, viability and colony-forming assays
  - Flow cytometric analyses
  - Genetic manipulation
  - Immunoblot analyses
  - Immunoprecipitation
  - Fluorescence microscopy analysis
  - Intracellular ATP quantification
  - Electron microscopy
  - qRT-PCR and mRNA stability
  - Polysome profiling
  - Mass spectrometry analysis
- QUANTIFICATION AND STATISTICAL ANALYSIS

SUPPLEMENTAL INFORMATION

Supplemental Information can be found online at https://doi.org/10.1016/j.celrep.2020.108162.

ACKNOWLEDGMENTS

We are particularly grateful to Federica Loro for administrative assistance; Maria Materozzi for the graphical abstract; Nicola Manfrini and Stefano Biffo for sharing early FAM46C-FNDC3 protein interaction data; Céline Schaeffer, Mirko Luoni, Vania Broccoli, Lynne Hocking, and Ineke Braakman for plasmids and antibodies; and Roberto Sitia, Giovanni Tonon, and all the Cenci lab members for fruitful discussions. We thank the ALEMBIC facility at San Raffaele Scientific Institute for microscopy analyses. MS analyses were performed at the Cogentech Proteomics/MS Facility or ProMiFa facility in Milan. This work was supported by grants to E.M. from the Multiple Myeloma Research Foundation (Research Fellow Award 2016), the International Myeloma Foundation (Brian D. Novis Junior Research Award 2019), Ospedale San Raffaele (5Xmille SEED), and Fondazione Cariplo (2018-0257) and by grants to S.C. from Fondazione AIRC (Investigator Grants 18858 and 23245) and Fondazione Cariplo (2018-0541).

AUTHOR CONTRIBUTIONS

Conceptualization, M.N., S.C., and E.M.; Methodology – Resources, U.O., F.P., A.R., E.P., and L.R.; Investigation, C.F., E. Riva, T.P., E. Ruggieri, M.R., F.C., and E.M.; Writing – Original Draft, S.C. and E.M.; Funding Acquisition, S.C. and E.M.; Supervision, S.C. and E.M.

DECLARATION OF INTERESTS

The authors declare no competing interests.

Received: February 13, 2020
Revised: June 23, 2020
Accepted: August 26, 2020
Published: September 22, 2020

Figure 7. Under Proteostatic Stress, p62 Diverts Excess FAM46C from FNDC3 Proteins through Its ZZ-Type Domain

(A) Co-immunoprecipitation of p62 and FNDC3 proteins with FLAG-FAM46C in RPMI 8226 cells under 1 μM Btz for 4 h.

(B) Immunofluorescence analysis of FLAG-FAM46C (red), p62 (green), and calnexin (cyan) in OPM2 cells treated with 1 μM Btz for 4h. Nuclei are stained blue with DAPI. Scale bars, 10 μm.

(C) Equal numbers of HeLa cells were seeded and stained after 5 days with crystal violet. Absorbance quantification after DMSO solubilization (mean ± SEM; two-way ANOVA with Bonferroni post hoc test versus mock cells, $^{**}p < 0.01$, $^{****}p < 0.0001$).

(D) Co-immunoprecipitation of FNDC3 proteins with FLAG-FAM46C in p62 WT and KO HeLa cells. Left: representative blots; right: quantification of FNDC3 band intensities normalized on FAM46C (mean ± SEM; n = 3; Welch's t test, $^{*}p < 0.05$).

(E) Co-immunoprecipitation analysis of HA-FAM46C with different mutants of FLAG-p62 in HeLa cells KO for endogenous p62 (ΔUBA, 1–395 aa; ΔZZ, Δ117–236 aa; PB1-ZZ, 1–192 aa).

(F) Co-immunoprecipitation analysis of endogenous FAM46C with p62 in RPMI 8226 cells under 1 μM Btz for 4 h with or without XRK3F2 10 μM for 1 h. Left: representative blots; right: quantification of FAM46C intensity normalized on p62 (mean ± SEM; n = 5; Welch's t test, $^{**}p < 0.01$).

(G) Immunoblot analysis in RPMI 8226 cells treated with the indicated doses of XRK3F2, bortezomib, or vehicle (DMSO) for 4 h. Left: representative blots; right: quantification of band intensities (mean ± SEM; n = 5; repeated-measures one-way ANOVA with Bonferroni post hoc test versus vehicle treated cells, $^{*}p < 0.05$, $^{**}p < 0.01$).

(H) Annexin V and propidium iodide staining of RPMI 8226 cells treated with XRK3F2 5μM, bortezomib 2.5 nM, or vehicle for 24 and 48 h. Quantification of positive cells (mean ± SEM; n = 6; one-way ANOVA with Bonferroni post hoc test versus vehicle treated cells, $^{*}p < 0.05$, $^{**}p < 0.01$, $^{****}p < 0.0001$).

See also Figure S7 and Data S3.

REFERENCES

Anderson, K.C. (2016). Progress and paradigms in multiple myeloma. Clin. Cancer Res. *22*, 5419–5427.

Barbariga, M., Vallone, F., Mosca, E., Bignami, F., Magagnotti, C., Fonteyne, P., Chiappori, F., Milanesi, L., Rama, P., Andolfo, A., and Ferrari, G. (2019). The role of extracellular matrix in mouse and human corneal neovascularization. Sci. Rep. *9*, 14272.

Barbieri, M., Manzoni, M., Fabris, S., Ciceri, G., Todoerti, K., Simeon, V., Musto, P., Cortelezzi, A., Baldini, L., Neri, A., and Lionetti, M. (2016). Compendium of FAM46C gene mutations in plasma cell dyscrasias. Br. J. Haematol. *174*, 642–645.

Battista, R.A., Resnati, M., Facchi, C., Ruggieri, E., Cremasco, F., Paradiso, F., Orfanelli, U., Giordano, L., Bussi, M., Cenci, S., and Milan, E. (2018). Autophagy mediates epithelial cancer chemoresistance by reducing p62/SQSTM1 accumulation. PLoS ONE *13*, e0201621.

Bell, J.L., Wächter, K., Mühleck, B., Pazaitis, N., Köhn, M., Lederer, M., and Hüttelmaier, S. (2013). Insulin-like growth factor 2 mRNA-binding proteins (IGF2BPs): post-transcriptional drivers of cancer progression? Cell. Mol. Life Sci. *70*, 2657–2675.

Bilska, A., Kusio-Kobiałka, M., Krawczyk, P.S., Gewartowska, O., Tarkowski, B., Kobyłecki, K., Nowis, D., Golab, J., Gruchota, J., Borsuk, E., et al. (2020). Immunoglobulin expression and the humoral immune response is regulated by the non-canonical poly(A) polymerase TENT5C. Nat. Commun. *11*, 2032.

Bolli, N., Biancon, G., Moarii, M., Gimondi, S., Li, Y., de Philippis, C., Maura, F., Sathiaseelan, V., Tai, Y.-T., Mudie, L., et al. (2018). Analysis of the genomic landscape of multiple myeloma highlights novel prognostic markers and disease subgroups. Leukemia *32*, 2604–2616.

Boyd, K.D., Ross, F.M., Walker, B.A., Wardell, C.P., Tapper, W.J., Chiecchio, L., Dagrada, G., Konn, Z.J., Gregory, W.M., Jackson, G.H., et al.; NCRI Haematology Oncology Studies Group (2011). Mapping of chromosome 1p deletions in myeloma identifies FAM46C at 1p12 and CDKN2C at 1p32.3 as being genes in regions associated with adverse survival. Clin. Cancer Res. *17*, 7776–7784.

Brewer, J.W., and Hendershot, L.M. (2005). Building an antibody factory: a job for the unfolded protein response. Nat. Immunol. *6*, 23–29.

Cenci, S. (2012). The proteasome in terminal plasma cell differentiation. Semin. Hematol. *49*, 215–222.

Cenci, S., van Anken, E., and Sitia, R. (2011). Proteostenosis and plasma cell pathophysiology. Curr. Opin. Cell Biol. *23*, 216–222.

Cenci, S., Oliva, L., Cerruti, F., Milan, E., Bianchi, G., Raule, M., Mezghrani, A., Pasqualetto, E., Sitia, R., and Cascio, P. (2012). Pivotal advance: protein synthesis modulates responsiveness of differentiating and malignant plasma cells to proteasome inhibitors. J. Leukoc. Biol. *92*, 921–931.

Cha-Molstad, H., Yu, J.E., Feng, Z., Lee, S.H., Kim, J.G., Yang, P., Han, B., Sung, K.W., Yoo, Y.D., Hwang, J., et al. (2017). p62/SQSTM1/Sequestosome-1 is an N-recognin of the N-end rule pathway which modulates autophagosome biogenesis. Nat. Commun. *8*, 102.

Chapman, M.A., Lawrence, M.S., Keats, J.J., Cibulskis, K., Sougnez, C., Schinzel, A.C., Harview, C.L., Brunet, J.-P., Ahmann, G.J., Adli, M., et al. (2011). Initial genome sequencing and analysis of multiple myeloma. Nature *471*, 467–472.

Chen, H., Lu, D., Shang, G., Gao, G., and Zhang, X. (2020). Structural and functional analyses of the FAM46C/Plk4 complex. Structure *28*, 910–921.e4.

Chou, T.C., and Martin, N. (2005). CompuSyn for drug combinations: PC software and user's guide: a computer program for quantitation of synergism and antagonism in drug combinations, and the determination of IC50 and ED50 and LD50 values. (Paramus, NJ: CompuSyn).

Diener, S., Bayer, S., Sabrautzki, S., Wieland, T., Mentrup, B., Przemeck, G.K.H., Rathkolb, B., Graf, E., Hans, W., Fuchs, H., et al. (2016). Exome sequencing identifies a nonsense mutation in Fam46a associated with bone abnormalities in a new mouse model for skeletal dysplasia. Mamm. Genome *27*, 111–121.

Doyard, M., Bacrot, S., Huber, C., Di Rocco, M., Goldenberg, A., Aglan, M.S., Brunelle, P., Temtamy, S., Michot, C., Otaify, G.A., et al. (2018). *FAM46A* mutations are responsible for autosomal recessive osteogenesis imperfecta. J. Med. Genet. *55*, 278–284.

Durán, A., Serrano, M., Leitges, M., Flores, J.M., Picard, S., Brown, J.P., Moscat, J., and Diaz-Meco, M.T. (2004). The atypical PKC-interacting protein p62 is an important mediator of RANK-activated osteoclastogenesis. Dev. Cell *6*, 303–309.

Fan, X., Chen, X., Deng, W., Zhong, G., Cai, Q., and Lin, T. (2013). Up-regulated microRNA-143 in cancer stem cells differentiation promotes prostate cancer cells metastasis by modulating FNDC3B expression. BMC Cancer *13*, 61.

Ghandi, M., Huang, F.W., Jané-Valbuena, J., Kryukov, G.V., Lo, C.C., McDonald, E.R., 3rd, Barretina, J., Gelfand, E.T., Bielski, C.M., Li, H., et al. (2019). Next-generation characterization of the Cancer Cell Line Encyclopedia. Nature *569*, 503–508.

Giannelli, S.G., Luoni, M., Castoldi, V., Massimino, L., Cabassi, T., Angeloni, D., Demontis, G.C., Leocani, L., Andreazzoli, M., and Broccoli, V. (2018). Cas9/sgRNA selective targeting of the P23H Rhodopsin mutant allele for treating retinitis pigmentosa by intravitreal AAV9.PHP.B-based delivery. Hum. Mol. Genet. *27*, 761–779.

Gross, E., Sevier, C.S., Heldman, N., Vitu, E., Bentzur, M., Kaiser, C.A., Thorpe, C., and Fass, D. (2006). Generating disulfides enzymatically: reaction products and electron acceptors of the endoplasmic reticulum thiol oxidase Ero1p. Proc. Natl. Acad. Sci. U S A *103*, 299–304.

Han, B., Wang, H., Zhang, J., and Tian, J. (2020). FNDC3B is associated with ER stress and poor prognosis in cervical cancer. Oncol. Lett. *19*, 406–414.

Haynes, C.M., Titus, E.A., and Cooper, A.A. (2004). Degradation of misfolded proteins prevents ER-derived oxidative stress and cell death. Mol. Cell *15*, 767–776.

Herrero, A.B., Quwaider, D., Corchete, L.A., Mateos, M.V., García-Sanz, R., and Gutiérrez, N.C. (2020). FAM46C controls antibody production by the polyadenylation of immunoglobulin mRNAs and inhibits cell migration in multiple myeloma. J. Cell. Mol. Med. *24*, 4171–4182.

Hoang, P.H., Dobbins, S.E., Cornish, A.J., Chubb, D., Law, P.J., Kaiser, M., and Houlston, R.S. (2018). Whole-genome sequencing of multiple myeloma reveals oncogenic pathways are targeted somatically through multiple mechanisms. Leukemia *32*, 2459–2470.

Huang, W., Sherman, B.T., and Lempicki, R.A. (2009). Systematic and integrative analysis of large gene lists using DAVID bioinformatics resources. Nat. Protoc. *4*, 44–57.

Klionsky, D.J., Abdelmohsen, K., Abe, A., Abedin, M.J., Abeliovich, H., Arozena, A.A., Adachi, H., Adams, C.M., Adams, P.D., Adeli, K., et al. (2016). Guidelines for the use and interpretation of assays for monitoring autophagy. Autophagy *8*, 445–544.

Kortüm, K.M., Langer, C., Monge, J., Bruins, L., Zhu, Y.X., Shi, C.X., Jedlowski, P., Egan, J.B., Ojha, J., Bullinger, L., et al. (2015). Longitudinal analysis of 25 sequential sample-pairs using a custom multiple myeloma mutation sequencing panel (M(3)P). Ann. Hematol. *94*, 1205–1211.

Kuchta, K., Muszewska, A., Knizewski, L., Steczkiewicz, K., Wyrwicz, L.S., Pawlowski, K., Rychlewski, L., and Ginalski, K. (2016). FAM46 proteins are novel eukaryotic non-canonical poly(A) polymerases. Nucleic Acids Res. *44*, 3534–3548.

Kwon, D.H., Park, O.H., Kim, L., Jung, Y.O., Park, Y., Jeong, H., Hyun, J., Kim, Y.K., and Song, H.K. (2018). Insights into degradation mechanism of N-end rule substrates by p62/SQSTM1 autophagy adapter. Nat. Commun. *9*, 3291.

Liang, T., Ye, X., Liu, Y., Qiu, X., Li, Z., Tian, B., and Yan, D. (2018). FAM46B inhibits cell proliferation and cell cycle progression in prostate cancer through ubiquitination of β-catenin. Exp. Mol. Med. *50*, 1–12.

Lin, C.-H., Lin, Y.-W., Chen, Y.-C., Liao, C.-C., Jou, Y.-S., Hsu, M.-T., and Chen, C.-F. (2016). FNDC3B promotes cell migration and tumor metastasis in hepatocellular carcinoma. Oncotarget *7*, 49498–49508.

Martins, G., and Calame, K. (2008). Regulation and functions of Blimp-1 in T and B lymphocytes. Annu. Rev. Immunol. *26*, 133–169.

Milan, E., Perini, T., Resnati, M., Orfanelli, U., Oliva, L., Raimondi, A., Cascio, P., Bachi, A., Marcatti, M., Ciceri, F., and Cenci, S. (2015). A plastic SQSTM1/p62-dependent autophagic reserve maintains proteostasis and determines proteasome inhibitor susceptibility in multiple myeloma cells. Autophagy *11*, 1161–1178.

Milan, E., Fabbri, M., and Cenci, S. (2016). Autophagy in plasma cell ontogeny and malignancy. J. Clin. Immunol. *36* (*Suppl 1*), 18–24.

Minnich, M., Tagoh, H., Bönelt, P., Axelsson, E., Fischer, M., Cebolla, B., Tarakhovsky, A., Nutt, S.L., Jaritz, M., and Busslinger, M. (2016). Multifunctional role of the transcription factor Blimp-1 in coordinating plasma cell differentiation. Nat. Immunol. *17*, 331–343.

Moscat, J., and Diaz-Meco, M.T. (2009). p62 at the crossroads of autophagy, apoptosis, and cancer. Cell *137*, 1001–1004.

Mroczek, S., Chlebowska, J., Kuliński, T.M., Gewartowska, O., Gruchota, J., Cysewski, D., Liudkovska, V., Borsuk, E., Nowis, D., and Dziembowski, A. (2017). The non-canonical poly(A) polymerase FAM46C acts as an onco-suppressor in multiple myeloma. Nat. Commun. *8*, 619.

Nutt, S.L., Taubenheim, N., Hasbold, J., Corcoran, L.M., and Hodgkin, P.D. (2011). The genetic network controlling plasma cell differentiation. Semin. Immunol. *23*, 341–349.

Nutt, S.L., Hodgkin, P.D., Tarlinton, D.M., and Corcoran, L.M. (2015). The generation of antibody-secreting plasma cells. Nat. Rev. Immunol. *15*, 160–171.

Obholz, K.L., Akopyan, A., Waymire, K.G., and MacGregor, G.R. (2006). FNDC3A is required for adhesion between spermatids and Sertoli cells. Dev. Biol. *298*, 498–513.

Palanichamy, J.K., Tran, T.M., Howard, J.M., Contreras, J.R., Fernando, T.R., Sterne-Weiler, T., Katzman, S., Toloue, M., Yan, W., Basso, G., et al. (2016). RNA-binding protein IGF2BP3 targeting of oncogenic transcripts promotes hematopoietic progenitor proliferation. J. Clin. Invest. *126*, 1495–1511.

Pengo, N., Scolari, M., Oliva, L., Milan, E., Mainoldi, F., Raimondi, A., Fagioli, C., Merlini, A., Mariani, E., Pasqualetto, E., et al. (2013). Plasma cells require autophagy for sustainable immunoglobulin production. Nat. Immunol. *14*, 298–305.

Pringle, E.S., McCormick, C., and Cheng, Z. (2019). Polysome profiling analysis of mRNA and associated proteins engaged in translation. Curr. Protoc. Mol. Biol. *125*, e79.

Richardson, P.G., Mitsiades, C., Hideshima, T., and Anderson, K.C. (2006). Bortezomib: proteasome inhibition as an effective anticancer therapy. Annu. Rev. Med. *57*, 33–47.

Rodriguez, A., Durán, A., Selloum, M., Champy, M.-F., Diez-Guerra, F.J., Flores, J.M., Serrano, M., Auwerx, J., Diaz-Meco, M.T., and Moscat, J. (2006). Mature-onset obesity and insulin resistance in mice deficient in the signaling adapter p62. Cell Metab. *3*, 211–222.

Sánchez-Martín, P., Saito, T., and Komatsu, M. (2019). p62/SQSTM1: 'Jack of all trades' in health and cancer. FEBS J. *286*, 8–23.

Sánchez-Martín, P., Sou, Y.S., Kageyama, S., Koike, M., Waguri, S., and Komatsu, M. (2020). NBR1-mediated p62-liquid droplets enhance the Keap1-Nrf2 system. EMBO Rep. *21*, e48902.

Schaeffer, C., Santambrogio, S., Perucca, S., Casari, G., and Rampoldi, L. (2009). Analysis of uromodulin polymerization provides new insights into the mechanisms regulating ZP domain-mediated protein assembly. Mol. Biol. Cell *20*, 589–599.

Schubert, U., Antón, L.C., Gibbs, J., Norbury, C.C., Yewdell, J.W., and Bennink, J.R. (2000). Rapid degradation of a large fraction of newly synthesized proteins by proteasomes. Nature *404*, 770–774.

Shalem, O., Sanjana, N.E., Hartenian, E., Shi, X., Scott, D.A., Mikkelson, T., Heckl, D., Ebert, B.L., Root, D.E., Doench, J.G., and Zhang, F. (2014). Genome-scale CRISPR-Cas9 knockout screening in human cells. Science *343*, 84–87.

Shapiro-Shelef, M., Lin, K.-I., McHeyzer-Williams, L.J., Liao, J., McHeyzer-Williams, M.G., and Calame, K. (2003). Blimp-1 is required for the formation of immunoglobulin secreting plasma cells and pre-plasma memory B cells. Immunity *19*, 607–620.

Shapiro-Shelef, M., Lin, K.-I., Savitsky, D., Liao, J., and Calame, K. (2005). Blimp-1 is required for maintenance of long-lived plasma cells in the bone marrow. J. Exp. Med. *202*, 1471–1476.

Shevchenko, A., Tomas, H., Havlis, J., Olsen, J.V., and Mann, M. (2006). In-gel digestion for mass spectrometric characterization of proteins and proteomes. Nat. Protoc. *1*, 2856–2860.

Shimizu, Y., and Hendershot, L.M. (2009). Oxidative folding: cellular strategies for dealing with the resultant equimolar production of reactive oxygen species. Antioxid. Redox Signal. *11*, 2317–2331.

Sitia, R., and Braakman, I. (2003). Quality control in the endoplasmic reticulum protein factory. Nature *426*, 891–894.

Tellier, J., Shi, W., Minnich, M., Liao, Y., Crawford, S., Smyth, G.K., Kallies, A., Busslinger, M., and Nutt, S.L. (2016). Blimp-1 controls plasma cell function through the regulation of immunoglobulin secretion and the unfolded protein response. Nat. Immunol. *17*, 323–330.

Teramachi, J., Silbermann, R., Yang, P., Zhao, W., Mohammad, K.S., Guo, J., Anderson, J.L., Zhou, D., Feng, R., Myint, K.Z., et al. (2016). Blocking the ZZ domain of sequestosome1/p62 suppresses myeloma growth and osteoclast formation in vitro and induces dramatic bone formation in myeloma-bearing bones in vivo. Leukemia *30*, 390–398.

Turner, C.A., Jr., Mack, D.H., and Davis, M.M. (1994). Blimp-1, a novel zinc finger-containing protein that can drive the maturation of B lymphocytes into immunoglobulin-secreting cells. Cell *77*, 297–306.

Uhlén, M., Fagerberg, L., Hallström, B.M., Lindskog, C., Oksvold, P., Mardinoglu, A., Sivertsson, Å., Kampf, C., Sjöstedt, E., Asplund, A., et al. (2015). Proteomics. Tissue-based map of the human proteome. Science *347*, 1260419.

Vogl, D.T., Stadtmauer, E.A., Tan, K.-S., Heitjan, D.F., Davis, L.E., Pontiggia, L., Rangwala, R., Piao, S., Chang, Y.C., Scott, E.C., et al. (2014). Combined autophagy and proteasome inhibition: a phase 1 trial of hydroxychloroquine and bortezomib in patients with relapsed/refractory myeloma. Autophagy *10*, 1380–1390.

Yang, L., Song, X., Zhu, J., Li, M., Ji, Y., Wu, F., Chen, Y., Cui, X., Hu, J., Wang, L., et al. (2017). Tumor suppressor microRNA-34a inhibits cell migration and invasion by targeting MMP-2/MMP-9/FNDC3B in esophageal squamous cell carcinoma. Int. J. Oncol. *51*, 378–388.

Yang, Y., Willis, T.L., Button, R.W., Strang, C.J., Fu, Y., Wen, X., Grayson, P.R.C., Evans, T., Sipthorpe, R.J., Roberts, S.L., et al. (2019). Cytoplasmic DAXX drives SQSTM1/p62 phase condensation to activate Nrf2-mediated stress response. Nat. Commun. *10*, 3759.

Yun, Z., Zhichao, J., Hao, Y., Ou, J., Ran, Y., Wen, D., and Qun, S. (2017). Targeting autophagy in multiple myeloma. Leuk. Res. *59*, 97–104.

Zheng, C., Ouyang, Y.-C., Jiang, B., Lin, X., Chen, J., Dong, M.-Z., Zhuang, X., Yuan, S., Sun, Q.-Y., and Han, C. (2019). Non-canonical RNA polyadenylation polymerase FAM46C is essential for fastening sperm head and flagellum in mice†. Biol. Reprod. *100*, 1673–1685.

Zhu, Y.X., Shi, C.-X., Bruins, L.A., Jedlowski, P., Wang, X., Kortüm, K.M., Luo, M., Ahmann, J.M., Braggio, E., and Stewart, A.K. (2017). Loss of *FAM46C* promotes cell survival in myeloma. Cancer Res. *77*, 4317–4327.

STAR★METHODS

KEY RESOURCES TABLE

REAGENT or RESOURCE	SOURCE	IDENTIFIER
Antibodies		
rabbit anti FAM46C/TENT5C	CUSABIO Technology LLC	Cat# CSB-PA736203LA01HU
mouse anti FLAG M2 antibody	Sigma-Aldrich	Cat# F1804; RRID:AB_262044
rabbit anti-FNDC3A	Novus Biological	Cat# NBP1-88809; RRID:AB_11024611
rabbit anti-FNDC3B	Novus Biological	Cat# NBP1-90495; RRID:AB_11034225
rabbit anti-FNDC3B	Abcam	Cat# ab135714
mouse anti-β-actin	Sigma-Aldrich	Cat# A5441; RRID:AB_476744
rabbit anti-Calreticulin/CRT	GeneTex	Cat# GTX111627; RRID:AB_11175861
rabbit anti Calnexin/CNX	Sigma-Aldrich	Cat# C4731; RRID:AB_476845
rabbit anti-ERGIC53	Sigma-Aldrich	Cat# E1031; RRID:AB_532237
rabbit anti-GAPDH	Santa Cruz Biotechnologies	Cat# sc-25778; RRID:AB_10167668
rabbit anti-lambda light chains	Dako	Cat# A0194
rabbit anti-H3	Abcam	Cat# ab1791; RRID:AB_302613
mouse anti phospho- IκBα (S32/36)	Cell Signaling Technology	Cat# 9246; RRID:AB_2267145
mouse anti IκBα	Cell Signaling Technology	Cat# 4814; RRID:AB_390781
rabbit anti-IRF4	GeneTex	Cat# GTX129135
rabbit anti-LC3A	Novus Biological	Cat# NB100-2331; RRID:AB_10001955
rabbit anti-LDHA	Sigma-Aldrich	Cat# SAB1100050; RRID:AB_10606873
rabbit anti-NF-κB p65	Cell Signaling Technology	Cat# 8242; RRID:AB_10859369
rabbit anti-PDI	Dr. Ineke Braakman Lab, Utrecht, NL	N/A
rabbit anti-PRDM1/Blimp-1	Cell Signaling Technology	Cat# 9115; RRID:AB_2169699
rabbit anti-PRDX4	AbFrontier	Cat# PA0009; RRID:AB_1620984
mouse anti-Ubiquitin monoclonal Ab (P4D1)	Santa Cruz Biotechnologies	Cat# sc-8017; RRID:AB_2762364
guinea pig anti-p62/SQSTM1 C-terminal	ProGen	Cat# GP62-C; RRID:AB_2687531
rabbit anti-p62/SQSTM1	Sigma-Aldrich	Cat# P0067; RRID:AB_1841064
mouse anti-p62/SQSTM1	Abnova	Cat# H00008878-M01; RRID:AB_437085
rabbit anti phospho-p62 S349	Cell Signaling Technology	Cat# 16177S; RRID:AB_2798758
rabbit anti phospho-p62 S403	Cell Signaling Technology	Cat# 39786S;RRID:AB_2799162
rabbit anti-DYKDDDDK	Cell Signaling Technology	Cat# 14793; RRID:AB_2572291
mouse anti-HA.11 antibody	BioLegend	Cat# 901514; RRID:AB_2565336
Alexa Fluor 647 anti-CD271	BioLegend	Cat# 345114; RRID:AB_2572059
Alexa Fluor 488 goat anti-guinea pig IgG	Life Technologies	Cat# A11073; RRID:AB_2534117
Alexa Fluor 488 goat anti-mouse IgG	Life Technologies	Cat# A11029; RRID:AB_2534088
Alexa Fluor 488 goat anti-rabbit IgG	Life Technologies	Cat# A11034; RRID:AB_2576217
Alexa Fluor 546 goat anti-mouse IgG	Life Technologies	Cat# A11030; RRID:AB_2534089
Alexa Fluor 546 goat anti-rabbit IgG	Life Technologies	Cat# A11010; RRID:AB_2534077
Alexa Fluor 647 goat anti-mouse IgG	Life Technologies	Cat# A21236; RRID:AB_2535805
Alexa Fluor 647 goat anti-rabbit IgG	Life Technologies	Cat# A21245; RRID:AB_2535813
Alexa Fluor 647 goat anti-guinea pig IgG	Life Technologies	Cat# A21450; RRID:AB_2735091
Anti-rabbit IgG, HRP-linked	Cell Signaling Technology	Cat# 7074; RRID:AB_2099233
Anti-mouse IgG, HRP-linked	Cell Signaling Technology	Cat# 7076; RRID:AB_330924
Chemicals, Peptides, and Recombinant Proteins		
Bortezomib	Cell Signaling Technologies	Cat# 2204
Bafilomycin-A1	AdipoGen Life Sciences	Cat# BVT0252-M001

(*Continued on next page*)

Continued

REAGENT or RESOURCE	SOURCE	IDENTIFIER
XRK3F2	ProbeChem	Cat# PC-61297
CM-H2DCFDA	Life Technologies	Cat# C6827
Actinomycin D	Thermo Fisher Scientific	Cat# A7592
Cyclohexymide	Sigma-Aldrich	Cat# C7698
Trypan Blue dye 0.40%	Bio-Rad	Cat# 1450013
Crystal Violet	Sigma-Aldrich	Cat# C3886
Dimethyl sulphoxide	VWR Life Science	Cat# 0231-500ML
2-hydroxyethylagarose	Sigma-Aldrich	Cat# A9414
Thiazolyl blue tetrazolium bromide	Sigma-Aldrich	Cat# M2128
Polybrene	Sigma-Aldrich	Cat# H9268
Puromycin	Sigma-Aldrich	Cat# P8833
Blastcidin S	Sigma-Aldrich	Cat# 203350
Lipofectamine 2000	Thermo Fisher	Cat# 11668030
Protease inhibitor cocktail	Roche	Cat# 05056489001
PhosSTOP phosphatase inhibitor	Sigma-Aldrich	Cat# 4906845001
Igepal CA-630	Sigma-Aldrich	Cat# I3021
Pierce Protein A Plus Agarose beads	Thermo Scientific	Cat# 22811
Protein G Agarose beads	Millipore	Cat# 16-266
Triton X-100	Sigma-Aldrich	Cat# X100
DAPI	Sigma-Aldrich	Cat# D9542
Osmium tetroxide	Electron Microscopy Science	Cat# 19140
Sodium cacodylate trihydrate	Sigma-Aldrich	Cat# C4945
Potassium ferrocyanide	Electron Microscopy Science	Cat# 20150
Uranyl acetate	Electron Microscopy Science	Cat# 22400
Embed-812 resin	Electron Microscopy Science	Cat# 14120
Lead citrate tribasic	Sigma-Aldrich	Cat# 15326
Lead acetate trihydrate	Sigma-Aldrich	Cat# 316512
Lead nitrate	Merck	Cat# 1073980100
Sodium citrate tribasic dehydrate	Sigma-Aldrich	Cat# S4641
TriFAST	Euroclone	Cat# EMR507100
SYBR green I master mix	Roche	Cat# 04887352001
iTaq Univer SYBR Green Supermix	Bio-Rad	Cat# 1725122
Rnasin RNase inhibitor	Promega	Cat# N251B
SILAC RPMI medium	Thermo Scientific	Cat# 88365
L-Lysine:2HCl Unlabeled	Cambridge Isotope Laboratories	Cat# ULM-8766
L-ARGININE:HCl Unlabeled	Cambridge Isotope Laboratories	Cat# ULM-8347
L-Lysine:2HCl (4,4,5,5-D4)	Cambridge Isotope Laboratories	Cat# DLM-2640
L-Arginine:HCl (13C6; 15N2)	Sigma-Aldrich	Cat# 643440
L-Lysine:2HCl (13C6; 15N2)	Cambridge Isotope Laboratories	Cat# CNLM-291
L-Arginine:HCl (13C6; 15N4)	Cambridge Isotope Laboratories	Cat# CNLM-539-H
DTT	Sigma-Aldrich	Cat# D9779
Iodoacetamide	Sigma-Aldrich	Cat# I1149
Trypsin sequencing grade	Roche	Cat# 11418475001
Brilliant Blue R	Sigma-Aldrich	Cat# B7920
Critical Commercial Assays		
Luminescent CellTiter-Glo assay	Promega	Cat# G7571
FITC Annexin V Apoptosis Detection Kit	BD PharmMingen	Cat# 556547
DC protein assay	Bio-Rad	Cat# 5000116

(*Continued on next page*)

Continued

REAGENT or RESOURCE	SOURCE	IDENTIFIER
Qproteome Cell compartment kit	QIAGEN	Cat# 37502
ImProm-II Reverse Transcriptase System	Promega	Cat# A3800
Deposited Data		
Original data are deposited at Mendeley Data	This Paper	https://doi.org/10.17632/bmztpgs2dj.1
Human Protein Atlas Dataset	Human Protein Atlas	http://www.proteinatlas.org; Uhlén et al., 2015
DepMap Portal	Broad Institute	https://depmap.org/; Ghandi et al., 2019
Experimental Models: Cell Lines		
HeLa	ATCC	RRID: CVCL_0030
HEK293T	ATCC	RRID: CVCL_0063
MM.1S	Dr. Giovanni Tonon Lab, San Raffaele Scientific Institute	RRID: CVCL_8792
OPM2	Dr. Giovanni Tonon Lab, San Raffaele Scientific Institute	RRID: CVCL_1625
RPMI 8226	Dr. Giovanni Tonon Lab, San Raffaele Scientific Institute	RRID: CVCL_0014
U266	Dr. Giovanni Tonon Lab, San Raffaele Scientific Institute	RRID: CVCL_0566
LP1	Dr. Giovanni Tonon Lab, San Raffaele Scientific Institute	RRID: CVCL_0012
Experimental Models: Organisms/Strains		
C57BL/6 wild-type mice	Charles River	C57BL/6
Oligonucleotides		
See qRT-PCR section for primer sequences		N/A
Recombinant DNA		
pLKO.1-puromycin Non-Mammalian shRNA	Sigma-Aldrich	SHC002
pLKO.1-puromycin shFAM46C 1	Sigma-Aldrich	TRCN0000168095
pLKO.1-puromycin shFAM46C 2	Sigma-Aldrich	TRCN0000166958
pLKO.2-puro shFNDC3B 1	Sigma-Aldrich	TRCN0000229811
pLKO.2-puro shFNDC3B 2	Sigma-Aldrich	TRCN0000229812
pLKO.2-puro shPRDM1 1	Sigma-Aldrich	TRCN0000235668
pLKO.2-puro shPRDM1 2	Sigma-Aldrich	TRCN0000235670
pLKO.2-tGFP Non-Mammalian shRNA control	This paper, generated from Sigma-Aldrich SHC202	N/A
pLKO.2-tGFP shFNDC3A 1	This paper, generated from Sigma-Aldrich TRCN0000338613	N/A
pLKO.2-tGFP shFNDC3A 2	This paper, generated from Sigma-Aldrich TRCN0000338554	N/A
Human C-term FLAG-FAM46A cDNA	Genscript	OHu17426D
Human C-term FLAG-FAM46B cDNA	Genscript	OHu17470D
Human C-term FLAG-FAM46C cDNA	Genscript	OHu30151D
Human C-term FLAG-FAM46D cDNA	Genscript	OHu19029D
Human C-term HA-FAM46C cDNA	Genscript	OHu30151C
Human N-term FLAG-p62 cDNA	Dr. Lynne Hocking Lab, University of Aberdeen	N/A
Human Uromodulin cDNA	Dr. Luca Rampoldi Lab (San Raffaele Scientific Institute)	Schaeffer et al., 2009
U6-promoter-filler-gRNAscaffold-Blast	Dr. Vania Broccoli Lab (San Raffaele Scientific Institute)	Giannelli et al., 2018
pCAG-spCas9-Puro	Dr. Vania Broccoli Lab (San Raffaele Scientific Institute)	Giannelli et al., 2018

(*Continued on next page*)

Continued

REAGENT or RESOURCE	SOURCE	IDENTIFIER
U6-promoter-p62sgRNA-Blast	This Paper	N/A
PGK-FLAG-p62 mutants-CD271	This Paper	N/A
PGK-FLAG-FAM46 cDNAs-CD271	This Paper	N/A
Software and Algorithms		
FCS Express 6 Flow Research Edition	De Novo Software	https://denovosoftware.com/
CRISPR design online tool	Dr Zhang lab, Broad Institute	https://zlab.bio/guide-design-resources
ImageJ software	NIH	https://imagej.nih.gov/ij/
Roche LC480 software	Roche	N/A
Bio-Rad CFX Maestro	Bio-Rad	https://www.bio-rad.com/it-it/product/cfx-maestro-software-for-cfx-real-time-pcr-instruments?ID=OKZP7E15
MaxQuant	Max Planck Institute of Biochemistry	https://www.maxquant.org/
Scaffold software version 4.7.5	Proteome Software Inc.	http://www.proteomesoftware.com/products/scaffold/
Proteome Discoverer Software	Thermo Fisher Scientific	https://www.thermofisher.com/us/en/home.html
MASCOT version 1.4.1.14	Matrix Science	http://www.matrixscience.com/
DAVID Gene Ontology tool 6.8	Laboratory of Immunopathogenesis and Bioinformatics	https://david.ncifcrf.gov/
Prism v6.0	GraphPad	https://www.graphpad.com/scientific-software/prism/
Compusyn	ComboSyn, Inc.	http://www.combosyn.com/
Perseus v.1.1.1.21	Max Planck Institute of Biochemistry	https://www.maxquant.org/perseus/

RESOURCE AVAILABILITY

Lead Contact

Further information and requests for resources and reagents should be directed to and will be fulfilled by the Lead Contact, Dr. Enrico Milan (milan.enrico@hsr.it).

Materials Availability

All unique/stable reagents generated in this study are available from the Lead Contact, Dr. Enrico Milan, upon request.

Data and Code Availability

Proteomic datasets are included in this publication as supplemental Excel files. Original/source data are available at Mendeley Data (https://doi.org/10.17632/bmztpgs2dj.1).

EXPERIMENTAL MODEL AND SUBJECT DETAILS

Cell lines

Human MM cell lines MM.1S (female), OPM2 (female), RPMI 8226 (male), U266 (male) and LP1 (female) were kindly provided by Dr. Giovanni Tonon, San Raffaele Scientific Institute. MM cells were cultured in RPMI media (GIBCO-Life Technologies, 61870) supplemented with 10% fetal bovine serum (Euroclone, ECS0180L), L-glutamine (2 mM; GIBCO-Life Technologies, 25030-024), penicillin (100 U/ml; GIBCO-Life Technologies, 15140-122), streptomycin (100 μg/ml; Lonza) and sodium pyruvate (1 mM; GIBCO-Life Technologies, 11360-039). All lines were genotyped as described in Milan et al. (2015), characterized for CD138/Syndecan-1 expression and Ig secretion. FAM46C gene was analyzed by Sanger sequencing to confirm the previously reported mutations in MM.1S and OPM2 cells (Chapman et al., 2011; Zhu et al., 2017).

HEK293T (female) and HeLa (female) cells were cultured in Dulbecco's modified Eagle's medium (DMEM, GIBCO-Life Technologies, 41965039) supplemented as described above for RPMI media. All lines were periodically tested for mycoplasma negativity.

Animal models

Primary murine PCs were obtained by LPS-stimulation of purified splenic B cells from both male and female 4-6 months old C57BL/6 wild-type mice (Charles River), as previously described in Pengo et al. (2013). Animal care and procedures were approved by the

Italian Ministry of Health and the Institutional Animal Care and Use Committee Office (IACUC) of San Raffaele Scientific Institute under protocol #708.

METHOD DETAILS

Proliferation, viability and colony-forming assays

Cell proliferation of MM lines was assessed by seeding equal numbers of cells in triplicate and by counting them upon Trypan Blue dye 0.40% (Bio-Rad, 1450013) staining with TC20 Automated cell counter (Bio-Rad) at the indicated days. Cell proliferation and viability of HeLa cells were measured seeding equal amounts of cells in different 96-well plates. At the indicated day one plate was fixed and stained with Crystal Violet 0,5% (Sigma-Aldrich, C-3886) in 20% methanol (Sigma-Aldrich, 32213). Stained cells were resuspended in DMSO (VWR Life Science, 0231-500ML) and absorbance was read at 550 nm with Multiskan Ascent (Thermo Labsystem).

To asses colony-forming capacity, RPMI 8226 cells were resuspended in RPMI complete medium with 0.4% 2-hydroxyethylagarose (Sigma-Aldrich, A9414) at a concentration of 5,000 cells/well and plated over a 0.8% agar layer in a 6-well plate and incubated for 21 d. Upon staining with thiazolyl blue tetrazolium bromide (Sigma-Aldrich, M2128) for 4 h, colonies containing at least 20 cells, as assessed by light microscopy, were counted.

Flow cytometric analyses

To analyze XRK3F2 (ProbeChem, PC-61297) and bortezomib (Cell Signaling Technologies, #2204) toxicity, RPMI 8226 cells were treated as indicated in the specific experiment and stained with Fluorescein isothiocyanate (FITC)-conjugated AnnexinV and propidium iodide following the manufacturer's instructions (BD PharmMingen, 556547). For total ROS analysis, MM cells were stained with CM-H2DCFDA 1μM (Life Technologies, C6827) for 30 minutes in PBS (Euroclone, ECB4004L). All data were obtained with Accuri C6 Flow Cytometer (BD biosciences) and analyzed using the FCS Express 6 Flow Research Edition (*De Novo* Software).

Genetic manipulation

Plasmids used are listed in the Key Resources Table. Lentiviral viruses to stably express anti-FAM46C, anti-PRDM1 anti-FNDC3A, anti-FNDC3B and control shRNAs were generated starting from Mission shRNAs (Sigma-Aldrich). Human C-term FLAG-FAM46 cDNAs and human C-term HA-FAM46C cDNA were cloned in a plasmid with a bidirectional human PGK promoter co-expressing the protein of interest and truncated human CD271. Mutants of p62 were cloned in the same plasmid and generated by specific PCR from human N-term FLAG-tagged p62 cDNA (kind gift from Lynne Hocking, University of Aberdeen).

Lentiviral vectors were packaged with Sigma-Aldrich Mission shRNAs or FLAG-proteins cDNA, pMD2-VSV-G, pMDLg/pRRE and pCMV-Rev plasmids in HEK293T cells for 14 h, then medium was replaced. 30 h after medium change cell supernatants were collected, ultra-centrifuged, filtered and added to MM cells with polybrene (3 μg/ml, Sigma-Aldrich, H9268) for 16 h. Transduced cells were selected for 48 h with 1 μg/ml puromycin (Sigma-Aldrich, P8833) for FAM46C, FNDC3B and PRDM1 shRNAs, while infection efficiency was determined analyzing GFP positivity for FNDC3A silenced cells. Lentiviral transduction of human cDNAs was assessed checking CD271 expression with an Alexa Fluor 647 anti-CD271 (BioLegend, 345114) using Accuri C6 Flow Cytometer (BD Biosciences).

cDNA of human wild-type uromodulin was cloned in pcDNA 3.1(+) (Thermo Fisher Scientific) and an HA tag was inserted after the leader peptide in between T26 and S27 in the protein sequence as described in Schaeffer et al. (2009). Stable populations were generated by transfecting HEK293T cells using lipofectamine 2000 (Thermo Fisher, 11668030) following the manufacturer's protocol. Selection was started 24 h after transfection by adding 0.25 mg/ml G418 for 1-2 weeks (Thermo Fisher Scientific, 10131035).

HeLa p62 Ko cells were obtain by CRISPR/Cas9 knockout by transfecting cells with U6-promoter-filler-gRNAscaffold-Blast and pCAG-spCas9-Puro plasmids (kind gift from Vania Broccoli, San Raffaele Scientific Institute, described in Giannelli et al., 2018). SgRNAs were designed using CRISPR design online tool (https://zlab.bio/guide-design-resources) to target exon I of *SQSTM1* gene and cloned following the strategy described in Shalem et al. (2014). Transfected cells were selected by puromycin and blasticidin (Sigma-Aldrich, 203350) and subcloned seeding them in a 96 well/plate at a concentration of half cell/well. p62 KO cells were screened by Exon I sequencing and immunoblot for p62 protein. sgRNA for p62: CGTTCGCTACAAAAGCCGCG;

Immunoblot analyses

Total cellular extracts were obtained by lysis in 150 mM NaCl, 10 mM Tris-HCl (pH 7.5), protease inhibitor cocktail (Roche, 05056489001), PhosSTOP phosphatase inhibitor (Sigma-Aldrich, 4906845001) and 1% SDS (Sigma-Aldrich, 05030). Genomic DNA was mechanically removed using 0,5ml Insumed syringes (PIC solution). To analyze Ig and uromodulin secretion, equal numbers of cells were seeded in Optimem medium (GIBCO-Life Technologies, 31985) for 4 h, then the supernatant was separately collected and cells were lysed as described above. For soluble fractions, cells were collected and lysed in 150 mM NaCl, 10 mM Tris-HCl (pH 7.5) and Igepal CA-630 1% (Sigma-Aldrich, I3021) supplemented with protease inhibitors, for 15 min on ice. Insoluble material was pelleted at 13000 g for 15 minutes and solubilized in 1% SDS lysis buffer. Cellular fractionations were performed with Qproteome cell compartment kit (QIAGEN, 37502) following manufacturer's instructions. Protein amounts were quantified by DC protein assay (Bio-Rad, 5000116) as described by manufacturer. Western blot were performed using 15-45 μg of protein lysate in 8%–15%

SDS-PAGE gels as described in Battista et al. (2018). In experiments analyzing soluble and insoluble fractions or cell compartment distribution, samples were loaded on a cell number basis. Antibodies used are listed in the Key Resources Table. Images were obtained using ChemiDoc-it (UVP) for HRP-conjugated secondary Ab or FLA9000 (FujiFilm) for Alexa Fluor conjugated secondary antibodies. Densitometric analysis was performed using ImageJ software (https://imagej.nih.gov/ij/).

Immunoprecipitation

Cells were lysed in 150 mM NaCl, 10 mM Tris-HCl (pH 7.5) and 1% Igepal CA-630 (Sigma-Aldrich, I3021), supplemented with protease inhibitors as described above, incubated for 15 min on ice. Nuclei and insoluble materials were pelleted at 1000 g for 15 min. For endogenous p62 immunoprecipitation, soluble material was quantified and 3-5 mg protein lysate was incubated for 16 h with: 1) 30 μl of Pierce Protein A Plus Agarose beads (Thermo Scientific, 22811) pre-conjugated with 5 μg of rabbit anti-p62 (Sigma-Aldrich, P0067) for SILAC analysis; or 2) 30 μl of protein G Agarose beads (Millipore, 16-266) pre-conjugated with 5 μg of mouse monoclonal anti-p62 antibody (Abnova, Cat# H00008878-M01) for FAM46C-p62 co-immunoprecipitation. For endogenous FNDC3B immunoprecipitation, lysates were incubated for 16 h with 30 μl of Pierce Protein A Plus Agarose beads (Thermo Scientific, 22811) pre-conjugated with 5 μg of rabbit anti-FNDC3B (Abcam, ab135714). For immunoprecipitation of FLAG-tagged FAM46 proteins and p62 mutants, lysates were incubated for 16h with 30 μl of protein G Agarose beads (Millipore, 16-266) pre-conjugated with 5 μg of mouse monoclonal FLAG M2 antibody (Sigma-Aldrich, F1804). Beads were washed 4 times in 150 mM NaCl, 10 mM Tris-HCl (pH 7.5), and resuspended in Laemmli Buffer for SDS-PAGE resolution.

Fluorescence microscopy analysis

HeLa, RPMI 8226 and OPM2 cells were seeded on slides (previously coated with poly-l-lysine for RPMI 8226 and OPM2), treated as indicated, fixed with 4% paraformaldehyde, and permeabilized with PBS 0.3% Triton X-100 (Sigma-Aldrich, X100). Cells were stained with guinea pig p62 antisera (1:500; Progen, GP62-C), mouse anti FLAG M2 antibody (1:100; Sigma-Aldrich, F1804), rabbit anti calnexin (1:400; Sigma-Aldrich, C4731), rabbit anti-FNDC3B (1:100; Novus Biological, NBP1-90495) washed in PBS, and stained depending on the experiment with different combinations of: Alexa Fluor 488 goat anti-guinea pig IgG (1:500; Life Technologies, A11073), Alexa Fluor 488 anti-mouse IgG (1:500; Life Technologies, A11029), Alexa Fluor 488 anti-rabbit IgG (1:500; Life Technologies, A11034), Alexa Fluor 546 goat anti-mouse IgG (1:500; Life Technologies, A11030), Alexa Fluor 546 goat anti-rabbit IgG (1:500; Life Technologies, A11010), Alexa Fluor 647 goat anti-mouse IgG (1:500; Life Technologies, A21236) and DAPI (Sigma-Aldrich, D9542). Images were collected with Leica TCS SP8 confocal microscope using a 63 × objective and a numerical aperture of 1.4.

Intracellular ATP quantification

Intracellular ATP was quantified with the luminescent CellTiter-Glo assay according to the manufacturer's instructions (Promega, G7571). For each condition, 10,000 living cells were plated in quadruplicate on white 96-well multi-well plates and were analyzed with a Victor plate reader (Perkin-Elmer).

Electron microscopy

MM cells were fixed with 2.5% glutaraldehyde (Sigma-Aldrich, G7776) in 100 mM cacodylate buffer pH 7.4 (Sigma-Aldrich, C4945) for 1 h at room temperature, postfixed with 1% osmium tetroxide (Electron Microscopy Science, 19140), 1.5% potassium ferrocyanide (Electron Microscopy Science, 20150) in 100 mM cacodylate buffer pH 7.4 for 1 h on ice, stained in 0.5% uranyl acetate (Electron Microscopy Science, 22400) 16h, dehydrated in increasing concentrations of ethanol (Sigma-Aldrich, 51976) and finally embedded in Embed-812 resin (Electron Microscopy Sciences, 14120). Samples were cured at 60°C in an oven for 48 h. Blocks were sectioned using a Leica EM UC7 ultramicrotome (Leica Microsystems). Ultrathin sections (70 nm) were contrasted with 2% uranyl acetate (Electron Microscopy Science, 22400) and Sato's lead solutions (lead citrate tribasic, Sigma-Aldrich, 15326; lead nitrate, Merck, 1073980100; lead acetate trihydrate (Sigma-Aldrich, 316512; sodium citrate tribasic dehydrate, Sigma-Aldrich, S4641) and observed with Talos 120C (FEI) electron microscope, images were acquired with a 4k × 4K Ceta CMOS camera (Thermo Fisher Scientific). Estimation of ER profile areas was calculate in ImageJ software by superimposing to images a grid of random points and counting the number of point intercepting ER membranes respect to the total number of point in the cell profiles excluding the nuclear area.

qRT-PCR and mRNA stability

RNA was extracted with TriFAST (Euroclone, EMR507100), 1000 ng RNA retro-transcribed with ImProm-II Reverse Transcriptase System (Promega, A3800), and cDNA corresponding to 5 ng of original RNA used as template in qPCR reactions. qPCRs were performed using SYBR green I master mix (Roche, 04887352001) on Roche LightCycler 480. Data were analyzed on Roche LC480 software with Advance Relative Quantification using human H3 and ACTB expression as normalizer.

mRNA stability was assessed treating MM cells with 10 μg/ml actinomycin D (ThermoFisher Scientific, A7592) for the indicated time. RNA was the extracted and cDNA obtained as indicated above. qPCR assays were performed using iTaq SYBR Green Supermix (Bio-Rad, 1725122) on Bio-Rad CFX96 PCR. Data were analyzed on Bio-Rad CFX Maestro software using 18S RNA as normalizer.

Primers used were:

18S/RNA18SN1: FW TAGAGGGACAAGTGGCGTTC; REV CGCTGAGCCAGTCAGTGT;
ACTB: FW CTTCGCGGGCGACGAT; REV CCACATAGGAATCCTTCTGACCCAT;
BIP/HSPA5: FW TAGCGTATGGTGCTGCTGTC ; REV TGACACCTCCCACAGTTTCA;
CNX/CANX: FW GTAGCCCTTCCTGTGTTCCT; REV TGACAGTGCCACCATCTTCT;
CHOP/DDIT3: FW GAGCTGGAACCTGAGGAGAGA; REV GCAGTTGGATCAGTCTGCTT;
ERGIC53/LMAN1: FW TCCGCAACAAACCCTATCCT; REV CGGCTCTTTTCCAGGTTCAG;
FAM46C/TENT5C: FW CAGGCATCAAAGTGCACGAC; REV AGCTTGTTCACACCCTCTGG;
FNDC3A: FW CCTGGATATGCCCCACAGGT; REV GGCGGCATCATAGTTGGGAC;
FNDC3B: FW ATGCCCCACTTGGTGAATGG; REV ACCTGGAGGCACATGAATGG;
GAPDH: FW CCACATCGCTCAGACACCAT; REV GTGACCAGGCGCCCAATAC;
GCLM: FW TCAGTCCTTGGAGTTGCACA; REV ACACAGCAGGAGGCAAGATT;
H3: FW GTGAAGAAACCTCATCGTTACAGGCCTGGT; REV CTGCAAAGCACCGATAGCTGCGCTCTGGAA;
HMOX1: FW GCAACCCGACAGCATGCCCC; REV CAGCGGGGCCCGTACCAGAA;
IRF4: FW CCGGAAATCCCGTACCAATG; REV ACCTTATGCTTGGCTCTGTGG;
MZB1: FW AAATCTGGCAAAGGCAGAGA; REV CTAAGTCCTGGGCCTGTGAG;
NQO1: FW GGAGAGTTTGCTTACACTTACGC; REV AGTGGTGATGGAAAGCACTGCCTTC;
p62/SQSTM1: FW GGGGCGCCCTGAGGAACAGA; REV CCTGGTGAGCCAGCCGCCTT;
PDI/P4HB: FW TCACATCCTGCTGTTCTTGC; REV GTCGCTGTCGATGAAGATGA;
PRDM1: FW CTGCGTGTCAGAACGGGATG; REV TGCTCGGTTGCTTTAGACTGC;
PRDX4: FW AACAGCTGTGATCGATGGAG; REV TCAAGTCTGTCGCCAAAAGC;
XBP1 spliced: FW CCGCAGCAGGTGCAGG; REV GAGTCAATACCGCCAGAATCCA;
XBP1 total: FW GCAAGCGACAGCGCCT; REV TTTTCAGTTTCCTCCTCAGCG;

Polysome profiling

Polysome profiling and RNA extraction from fractions were performed following the protocol reported in Pringle et al. (2019). Briefly, mock and FAM46C expressing OPM2 cells were counted and the same amount of cells was treated with 100 μg/ml cycloheximide (Sigma-Aldrich, C7698) for 3 min. Cells were lysed in 300 mM NaCl, 20 mM Tris-HCl (pH 7.5), 10 mM MgCl2, 100 μg/ml cycloheximide, RNase Inhibitor (Promega, N251B) and 1% Igepal CA-630 (Sigma-Aldrich, I3021), supplemented with protease and phosphatase inhibitors as described above, incubated for 15 min on ice. Nuclei and insoluble materials were pelleted at 13000 g for 15 min. Lysates were loaded on top of a 7%–47% sucrose linear gradient containing 100 μg/ml cycloheximide and centrifuged at 39,000 rpm on a SW 41 rotor (Beckman Coulter) for 90 min. UV absorbance was measured with Bio-Rad Automated Econo System (Bio-Rad), 1ml fractions were collected and RNA re-quantified with NanoDrop 8000 (Thermo Scientific). 500 μl of the indicated fractions were mixed 1:1 with TriFAST (Euroclone, EMR507100) and RNA extracted as described in the previous section. qPCRs were performed using SYBR green I master mix (Roche, 04887352001) on Roche LightCycler 480. Data were analyzed on Roche LC480 software with Advance Relative Quantification using 18S RNA as normalizer.

Mass spectrometry analysis

Analysis of p62 interactors upon bortezomib was performed as describes in Milan et al. (2015). Immunoprecipitation of FLAG-FAM46C was performed in OPM2 and LP1 cells with mouse monoclonal FLAG M2 antibody (Sigma-Aldrich, F1804) as described in the dedicated section. For SILAC analysis of FAM46C knockdown, FAM46C silenced (sh1 and sh2) and mock control RPMI 8226 cells were grown in complete SILAC RPMI medium (Thermo Scientific, 88365) supplemented with "light" (Lys0, Arg0; Cambridge Isotope Laboratories, ULM-8766 and ULM-8347), "intermediate" (Ly4, Arg6; Cambridge Isotope Laboratories, DLM-2640, Sigma-Aldrich, 643440) or "heavy" (Lys8, Arg10; Cambridge Isotope Laboratories, CNLM-291 and CNLM-539-H) amino acids. After 14d an incorporation test was performed to confirm labeling, then cells were mixed 1:1:1 inverting the labeling strategy (Mix1: mock light, sh1 intermediate, sh2 heavy; Mix2: mock heavy, sh1 intermediate, sh2 heavy). For label-free analysis of FAM46C effects, FAM46C overexpressing and mock OPM2 cells were collected 4 days after infection. For both experiments, MM cells were lysed in 150 mM NaCl, 10 mM Tris-HCl (pH 7.5), protease inhibitor cocktail (Roche, 05056489001) and 1% SDS (Sigma-Aldrich, 05030). Genomic DNA was mechanically removed using 0,5ml Insumed syringes (PIC solution). Immunoprecipitated proteins or 60μg of total protein lysate were loaded in a 4%–20% gradient SDS-PAGE and stained with Coomassie Brilliant Blue (Sigma-Aldrich, B7920). Gel slices sampling the entire length of the lanes were excised and processed as described in Shevchenko et al. (2006).

After reduction with 10mM DTT (Sigma-Aldrich, D9779), alkylation with 55 mM iodoacetamide (Sigma-Aldrich, I1149) and overnight digestion with trypsin 10ng/μl (Roche, 11418475001), tryptic peptides were desalted and concentrated on C18 Stage Tips (Proxeon Biosystems, SP301) following the manufacturer's instructions, and analyzed by LC-MS/MS with a Q-Exactive mass Spectrometer (Thermo Fisher Scientific) as described in Barbariga et al. (2019). Technical replicates were performed on the LC-MS/MS part of the analysis. For the identification of FAM46C interactors, raw files were analyzed with the Proteome Discoverer Software (Thermo Fisher Scientific) using MASCOT (Matrix Science version 1.4.1.14) as search engine. MS/MS based peptide and protein identifications were validated using Scaffold software (Proteome Software Inc., version 4.7.5). Identifications were accepted only for peptides and proteins with a probability greater than 95% and 99% respectively, calculated by the Scaffold Local FDR algorithm.

Validated proteins must contain at least 2 identified peptides. For full lysates proteomic analyses, raw data were processed with MaxQuant (version 1.5.2.8 for SILAC experiment, version 1.6.1.0 for label-free) and peptides identified from MS/MS spectra against the Human Uniprot Complete Proteome Set database (ver. 2017_07 for SILAC, ver. 2019_7 for label-free) using the Andromeda search engine. Cysteine carbamidomethylation was used as fixed modification, methionine oxidation and protein N-terminal acetylation as variable modifications. Mass deviation for MS/MS peaks was set at 0.5 m/z units and the peptides and protein false discovery rates (FDR) were set to 0.01. The minimal length required for a peptide was six amino acids; minimum two peptides and at least one unique peptide were required for high-confidence protein identification.

QUANTIFICATION AND STATISTICAL ANALYSIS

Graphs and data analysis were obtained using Prism v6.0 software (GraphPad). Statistical significance was tested as indicated in the figure legends. Asterisks indicate the following *p* values: *$p < 0.05$; **$p < 0.01$; ***$p < 0.001$; ****$p < 0.0001$. Figures were assembled with Adobe Illustrator. For mass spectrometry, the Perseus software (v.1.1.1.21) was used. Identification of significant protein changes required: i) significance B at $p < 0.05$; ii) $\geq$ 2 ratio counts iii) ratios concordant for both shRNAs in direct and reverse experiments. Proteins significantly modulated by FAM46C were run through functional annotation clustering on DAVID web resource, as described (Huang et al., 2009), using the list of quantified proteins as background, and UP_keyword, GOterm-BP-FAT, GO-term-CC-FAT, GOterm-MF-FAT and KEGG_pathways as search parameters. Cell compartment analysis was performed using the following categories: (Nucleus GO:0005634; Cytosol GO:0005829; Mitochondria GO:0005739; Ribosome GO: 0005840; ER GO:0005783; ERGIC GO:0033116; Golgi GO:0005794; Lysosome GO:0005764). The identification of FAM46C interactors was validated using Scaffold Software (Proteome Software Inc., version 4.7.5) as described in the dedicated section. Chou-Talalay test was performed using Compusyn software (ComboSyn, Inc; Chou and Martin, 2005).